Applied Energy 342 (2023) 121192

Contents lists available at ScienceDirect

Applied Energy

journal homepage: www.elsevier.com/locate/apenergy

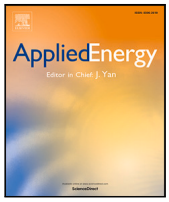

Analysis of energy variability and costs for offshore wind and hybrid power unit with equivalent energy storage system

Qiang Gao [a,*], Rui Yuan [a], Nesimi Ertugrul [a], Boyin Ding [a], Jennifer A. Hayward [b], Ye Li [c]

[a] School of Electrical and Mechanical Engineering, The University of Adelaide, Adelaide, Australia
[b] Energy Centre, Commonwealth Scientific and Industrial Research Organization, Newcastle, Australia
[c] School of Naval Architecture, Ocean and Civil Engineering, Shanghai Jiao Tong University, Shanghai, China

ARTICLE INFO

Keywords:
Wind energy
Wave energy
Hybrid system
Energy variability
Energy storage system
Techno-economic analysis

ABSTRACT

Offshore wind and wave energy are largely untapped renewable resources. However, the intermittency and the high cost of energy of these resources pose a few major challenges for their wide-scale developments. Although energy storage systems are considered to mitigate or reduce the energy variability to support a reliable power network, the proposed solutions have further increased the capital expenditure. This is primarily due to a lack of systematic techno-economic assessments of offshore renewable systems with energy storage. In addition, the integration of offshore wind and wave energy systems reported in previous literature showed a number of benefits, such as power smoothing and cost reduction. This paper investigates the offshore wind and wave energy intermittency and their dispatchability and proposes an equivalent energy storage system to achieve the same level of energy variability as the combined wind and wave system. This provides a thorough understanding of the power smoothing performance and firmness of energy supply in an offshore energy farm. The economic assessment of the stand-alone offshore wind system, the wind turbine with an energy storage system and the hybrid power unit system are conducted and compared via high-fidelity cost models. In addition, the sensitivities of three system configurations are investigated at multiple locations around the world, which are selected to address typical wind and sea states. The results indicate that the hybrid wind and wave power system has merits in reducing energy variability and enhancing ocean energy dispatchability while offering highly competitive cost, compared to the other two system configurations. Furthermore, the research aims to provide a guidance and support for the developers, investors and policymakers at the pre-planning stage of developing ocean renewable energy systems.

1. Introduction

Offshore wind and wave energy are two abundant ocean renewables at the forefront of the energy transition from fossil fuels to a carbon-free renewable energy future. Compared to the onshore wind, offshore wind presents significant benefits including stronger and steadier wind resources, which are vital to building larger wind turbines (WTs). Moreover, offshore wind farm development potentially has less conflict over land/space use and better community acceptance. Therefore, over the past decade, the offshore wind industry has grown significantly with installed capacity increasing by 21% every year since 2013. The total installed capacity has reached 35.3 GW by the end of 2020, which is projected to reach 200 GW by 2030 [1].

On the other hand, wave energy has a significant renewable energy potential as high as 2 TW globally. Since it is recognized as a more predictable resource than wind energy [2], there has been great interest from research institutions and industry. Therefore, a large number of wave energy converters (WECs) have been developed and proposed. However, a varying degree of achievements has been reported about WECs, from a prototype with limited experimental verification to a small-scale demonstration unit by industry [3,4]. However, no fully commercial wave farm has been deployed on a large scale, which is due to the high cost and complexity of the proposed systems.

1.1. Main challenges of developing offshore wind and wave energy

Two main challenges about the commercialization of offshore wind and wave energy systems are the high level of energy intermittency and their high levelized cost of energy (LCOE). Energy intermittency and variability are highly critical as more variable renewable energy resources are integrated into the conventional power grid that demands firmness with dispatchable energy resources [5]. Therefore, the energy

* Corresponding author.
E-mail address: qiang.gao@adelaide.edu.au (Q. Gao).

https://doi.org/10.1016/j.apenergy.2023.121192
Received 22 November 2022; Received in revised form 13 April 2023; Accepted 21 April 2023
Available online 4 May 2023

fluctuation in energy supply, ramps, creates challenges for maintaining the supply–demand balance and threatens the power system security as well as reliability, as a form of uncertainty [6,7]. In addition, large ramps in wind power are difficult to manage [8,9] and understanding ramp events is critical. This is required for wind power operators, utilities as well as system operators to be able to set informative strategies for electricity demand and generation balance, as well as for economical and environmental benefits [8,10].

In recent years, energy storage systems (ESSs) have been considered as a solution to reduce the intermittency in the wind and solar renewable resources. Therefore, different energy storage technologies are considered, including mechanical energy storage systems (such as flywheel [11,12] and compressed air [13]), electrical storage systems (such as batteries [14] and super-capacitors [15]) and other types of energy storage systems (such as hydrogen, biomass and thermal energy storage reported in [16]). However, the deployment of any ESS depends on the specific charging/discharging characteristics of the technology, its primary and secondary purposes in the power network and the specific application (such as in an onshore or an offshore farm).

The second major barrier to the development of commercial offshore wind and wave farms is the relatively high cost (usually LCOE) compared with other decarbonization options, such as onshore wind and solar energy [17], which are mainly due to the harsh hydrodynamics environment [18,19]. For example, the cost of offshore wind turbines and foundations are more expensive than the onshore counterparts, by 20% and 350%, respectively [20]. Similar to onshore wind turbines, distance between turbines within an offshore wind farm significantly affects the operational and maintenance cost considering the aerodynamics challenges [21,22], while its optimal distance is more difficult to obtain compared with onshore farm due to the challenging hydrodynamics problem [23]. These result in an average LCOE of about 77 $/MWh for fixed-bottom offshore wind farms [24] and 97 $/MWh for floating wind farms [25], compared to the 33–34 $/MWh for onshore wind farms [24,26]. In terms of wave energy, the lack of convergence towards a mature WEC farm design prohibits their further development and significant capital expenditure is needed [27]. Therefore, in recent wave energy projects, LCOE is found above 300 $/MWh [28,29]. As the focus of this study is at the system level, we would not discuss the hydrodynamics and aerodynamics challenges in greater detail.

1.2. Development of integrated wind and wave energy

The integration of offshore wind and wave energy systems is emerging aimed to capture largely untapped ocean renewables. Based on the degree of system connectivity [2,30], the combined energy farm can be categorized by two types: co-located system and hybrid system. The co-located wind and wave farm shares the common grid transmission infrastructure in the same marine area. The hybrid system is designed to accommodate both offshore WT and WEC on a single platform which could further reduce the overall cost as multiple system components are shared. However, the interaction between WT and WEC and the platform stability becomes critical.

Therefore, the hydrodynamic responses of such hybrid systems have been investigated in previous studies. For example, a hybrid offshore wind and wave energy converter with a monopile substructure is investigated aiming to prove the viability of the proposed hybrid solution based on the experimental analysis of the hydrodynamic response of the WEC subsystem [31]. Michele et al. developed a hydrodynamic model of the oscillating water column in a hybrid offshore wind and wave system to investigate the impact of the skirt height and opening angles on the hydrodynamic behaviour and system efficiency [32]. The analysis results of the analytical model are validated by the experimental setups. A hybrid wind and wave system is proposed in the study [33] by integrating a semi-submersible floating WT with three point absorber WECs. Different WEC power-take-off control strategies are compared and their results indicate that, in general, reactive control worsens the hybrid platform dynamics but leads to the highest wave power generation. The spring-damping control shows better mitigation of the pitch motion of the platform but almost half power generation as much as reactive control. In study [34], Fantai et al. proposed a novel control framework via two-stage model predictive control for investigating the hydrodynamic of combining a floating offshore WT with a small WEC array. Their results demonstrated that the motion suppression and power reliability of a floating offshore WT can be simultaneously achieved by using co-located WECs.

It was also shown in the previous studies that, the combined offshore wind and wave energy conversion systems have clear benefits compared to the standalone system either only WT or only WEC. First, the combined system significantly reduces energy intermittency and variability. For example, Gao et al. studied the short-term power intermittency (seconds to mins) between a hybrid system and a standalone WT system and results show an average of 40% reduction in short-term power fluctuation [35]. Astariz et al. investigated the energy variability and downtime of a combined offshore wind and wave farm and their results indicate that up to 87% of downtime reductions and 6% energy variability reduction can be achieved by a combined system, respectively [36]. By analysing hourly and diurnal variability indexes, the power output variability for collocating offshore wind and wave generations is studied in multiple sites throughout the US East and West Coasts and the UK North Sea [37]. It is also found that the benefits of power variability reduction differ regionally and should be assessed locally.

In addition, the combined system has other unique advantages [38] in cost reduction (usually in LCOE) of an offshore energy farm due to the shared expensive infrastructure and operation and maintenance [39,40], and enhancement of the energy production [41].

It should be noted here that the advantage of the combined systems in the reduction of energy variability has been investigated and approved by previous works [36,42]. However, such analyses in most studies were primarily focused on the modelling and analysis of various energy variability indexes, such as coefficient of variability, temporal and spatial variations and the correlation between wind and wave energy generation [43]. Generally, purely statistical analysis of variability reduction is not straightforward to understand the energy smoothing effect of a hybrid system for integration with the common grid. In other words, a reduction of 20% in the energy variability index does not have practical meaning in technical aspects such as power generation, dispatch and economic aspects, such as those directly related to the costs or revenues. Therefore, a realistic and practical justification is needed to support the statistical conclusions obtained from the variability indexes. In addition, previous economic analyses in [44] and comparison study in [45] between the offshore wind farm and the combined energy farm have not considered the energy farm dispatchability (in relation to the local energy demand), power generation ramps events and their associated system costs. Since these criteria can affect the final offshore energy farm configurations, the different potential system configurations should be studied systematically and compared in terms of energy dispatchability using techno-economical assessment.

1.3. Objective of this research

To address the above research gaps and clearly understand technical and economic synergies in a combined energy farm, this paper proposes a novel "virtual energy storage" concept to quantitatively justify the energy variability reduction performance, energy farm dispatchability, and associated costs. Then, different energy farm configurations, such as the standalone WT, the WT with equivalent energy storage system (WTESS) and the hybrid wind and wave power unit (HPU), are studied and compared by developing an integrated techno-economic assessment approach. This study also investigates and compares the power ramping characteristics (seasonally patterns, ramp duration) between

HPU and WT and the cost–benefit between the HPU and WTESS under the same variability conditions. Note that another novelty of this paper is to develop an integrated techno-economic assessment method for the hybrid systems and the synergies between each other. Moreover, multiple sea locations with various resource characteristics around the world are studied to understand the sensitivity of results to the wave resource types.

This paper is structured as follows: Section 2 introduces the data collection, energy assessment and three offshore system configurations. In Section 3, the technical assessment of offshore energy farms is conducted, including energy variability characterization and ESS sizing. High-fidelity life cycle cost models are developed in Section 4 to assess the economic feasibility of various offshore energy farms. Section 5 discusses the techno-economic sensitivity of system configurations under specific wave characteristics and locations. Conclusions are drawn in Section 6.

2. Wind and wave sources and systems description

2.1. Site selection and specification

In order to assess the energy generation variability and costs of various system configurations and to cover the wind and wave climate diversities, 5 different sites were selected, covering the locations in the Northern and the Southern hemispheres. These include three sites in the Australian coastal region (Sydney, Port Lincoln and Cliff Head), one site in the North Sea and one site in the Western coast of North American (Blunt Reef), which are based on the studies reported in [43,46,47]. Note that, these sites cover all wave types defined in the literature, including swell wave, wind-wave and mixed wave types, which are sensitive to the combined energy farm generation performance [43].

A wind-wave hindcast undertaken by the Center for Australian Weather and Climate Research (CAWCR) with attention focused on Australian domains is used in this paper [48]. This hindcast data operates on a series of nested grids of 4 arcminutes (~7 km) in Australian regions and has been validated by in-situ wave buoy and satellite altimeter observations [49]. The resource data of Europe and the US used in this paper are obtained from ERA5 [50] data, which is reanalysis data running at hourly resolution with nested grids of 0.25 degrees (~27 km). It provides a large number of atmospheric, ocean-wave and land-surface quantities. The main parameters of the data-set considered in this paper include the wind speed at 10 m or/and 100 m height, significant wave height, wave peak period, wave energy flux and the bathymetry. Note that, although a few locations with distinct resource characteristics are discussed in this paper, the method of analysis can be adapted to other sea locations. Note also that one sea site close to the Sydney location is systematically studied in Sections 3–4 and the sensitivity study on multiple other locations are discussed in Section 5.

2.2. Method of energy resources assessment

It is known that the wind power density (P_{wind}) is proportional to the cube of the wind speed (v_w) at hub height, given by:

$$P_{wind} = \frac{1}{2}\rho_a v_w^3. \tag{1}$$

where ρ_a is the air density (assuming 1.15 kg/m^3 at 15 °C) at hub height. To characterize the impact of the height and the roughness of the blowing surface on wind speed, v_w can be estimated by:

$$v_w = U_{10} \cdot \left(\frac{z_{100}}{z_{10}}\right)^{\alpha}, \tag{2}$$

Here, z_{100} represents the hub height of 100 m; U_{10} is the wind speed at a reference height of 10 m (z_{10}); and α is the friction coefficient and a value of 0.1 is used under open water terrain [51].

The power density (power per unit of crest width, kw/m) of irregular wave (P_{wave}) can be defined based on the linear wave theory and assumption of deep water [49], given by:

$$P_{wave} = \frac{\rho_w g^2}{64\pi} H_s^2 T_e \tag{3}$$

where H_s and T_e are the significant wave height and wave energy period ($T_e = 0.857T_p$). ρ_w and g are the water density and gravity acceleration constant respectively.

Due to the synergies between wind and wave resources, it is possible to quantify their correspondence by Pearson cross-correlation given by Eq. (4) on an hourly basis.

$$C(\tau) = \frac{1}{N}\sum_{k=1}^{N-\tau} \frac{\left[x(k)-\mu_x\right]\cdot\left[y(k+\tau)-\mu_y\right]}{\sigma_x\sigma_y}, \tag{4}$$

N is the length of sample data and τ is the lag time between wind power density (x) and wave power density (y). $C(0)$ illustrates the instantaneous correlation between them and $C(\tau) = 0$ denotes no correspondence and $C(\tau) = 1$ represents a strong correlation. μ_x, μ_y and σ_x, σ_y are the mean value and standard deviation of wind and wave power densities, respectively.

2.3. System configurations

As it is mentioned in Section 1.3, three system conversion systems are described in this section. The direct-drive WT are considered in this paper (see Fig. 1a), which eliminates the gearbox hence greatly reducing the risk of drive-train failure and minimizing the associated operation and maintenance cost and energy loss of the WT. Note that this is critical specifically for the future offshore WT with a limited access time window.

The configuration of WTESS is shown in Fig. 1b and the ESS is divided into two parts: power unit (such as power electronics) and energy unit (for energy storage). The basic conversion principle of WEC is given in Fig. 1c. Note that the buoy and the PTO system convert the kinetic energy in the accident wave to mechanical energy in the form of shaft power which is coupled with the conventional rotating generator.

The layout of the hybrid power unit (HPU), which integrates one WT with four WECs, is displayed in Fig. 1e. Note that four WECs are evenly distributed around WT with a distance of 300 m to reduce the interactions between conversion devices. WEC power is delivered to the common coupling point at the WT platform via WEC-to-WT cables. In addition, the power of the HPU is transformed to the offshore substation via inter-array DC cable. This paper assumes that the WT and the WECs in this HPU (a co-located scheme) are working independently. In other words, each generation unit works on its own maximum power generation (according to its power curve and power matrix). It is also noted that the priority of power generation from various renewables could be an interesting topic especially when wind and wave resources or system capacity are unbalanced, and it can be achieved by specific control strategies.

As it is illustrated in Fig. 1, a directly driven brushless permanent magnet synchronous generator (PMSG) is considered with a DC–DC converter that is easily integrated into an ESS or a WEC [11,30] to provide a common coupling point for a DC link within and among the hybrid power units. Fig. 1b shows the WT with distributed ESS (WTESS) (located at the WT platform). The rotor side converter (RSC) is required to achieve maximum power tracking, and the grid side converter (GSC) is required for the main grid connection either at the offshore or onshore substations.

It is observed that the AC transmission system is the best economical option for a distance shorter than 50 km. If the distance is above this range, the DC transmission becomes a better option. It can be highlighted here that the DC system proposed in this work is an ideal solution for both inter-array cables (between WECs and WT in an HPU) and transmission cables [52]. This is due to the fact that

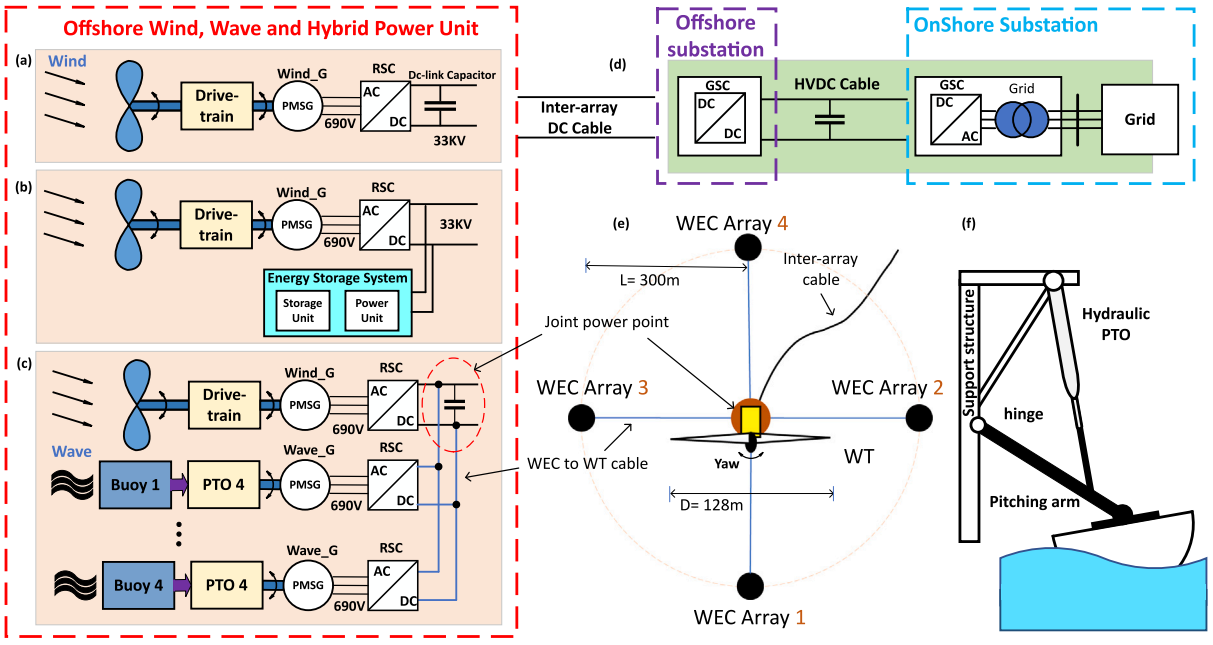

Fig. 1. System diagram of: (a) WT, (b) WTESS, (c) HPU, (d) Transmission topology, (e) the top view of HPU and (f) a general concept of point absorber WEC.

this arrangement reduces the number of power conversion systems (inverter and transformer) and avoids the issues associated with the long AC transmission lines and the coupling subsystems operating at different frequencies. Therefore, the DC-linked system is considered as a potential solution for the WT system and its hybridization with WEC.

2.4. Component selection and power calculation

The power generation of wind and wave can be estimated by the WT and WEC model with given the wind speed at hub height and wave statistics. The power curve of a WT turbine and the power matrix of a WEC have been widely used to assess the energy availability, variability and economic analysis for offshore energy farms [43,47,53,54], to avoid costly simulation studies and to obtain a quick assessment.

As a benchmark in this paper, a commercial WT (Gamesa G128-5 MW [41,55]) is selected. This turbine is suitable for deployment both in onshore and offshore farms [56] and its power curve is given in Fig. 2.

Regarding selecting WEC types, a large number of designs are proposed in the past decades [30], such as point absorbers, attenuators, over-toppings and oscillating water columns. In this paper, the point absorber prototype is selected as this type has been deployed in the open sea and was tested in a laboratory platform [57,58]. More specifically, a typical top-mounted pitching device [59] is used (see Fig. 1f) which was inspired by WaveStar [60]. Note that, the PA WEC system generally comprises three subsystems: the wave capturing system (such as the oscillating buoys in Fig. 1f), the hydraulic power-take-off system and the electrical conversion system. Here, the oscillating buoys are designed to convert the incident wave energy to kinetic energy in a hydraulic piston and the hydraulic PTO system can convert the piston power into mechanical power to drive the generator (rotatory or linear types) for electricity production. The similar detailed working principles of hydraulic PTO and generator can be found in the study [11]. In this paper, WaveStar C6 600 kW is selected as a reference WEC and its power matrix is given in Fig. 2 bottom, which has a technology level of TRL7 [60,61].

Note that the hydrodynamic analysis of foundation types applied to the WT is out of the scope of this study. Therefore, the impact of the platform on the WT power curve is ignored. Note also that the direction information plays an important role in power generation for both WT and WEC. Therefore, due to the symmetry of the WEC buoy and ideal yaw system in WT, the energy system components are considered to capture wind and wave energy from all directions.

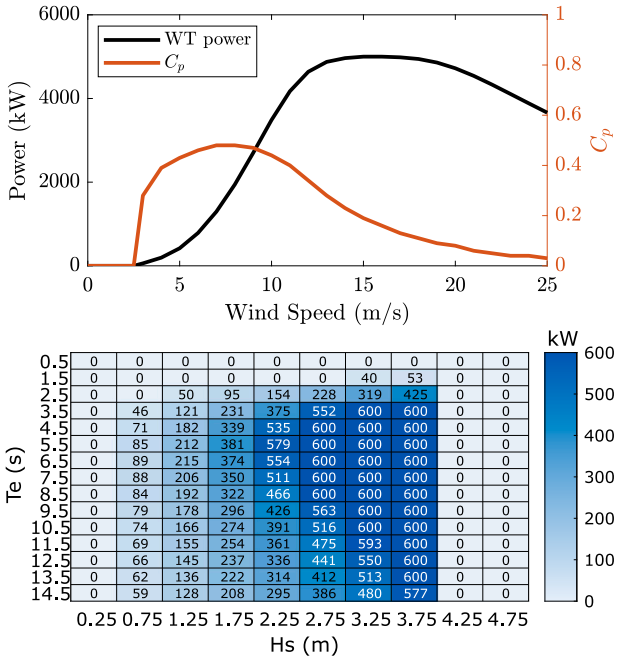

Fig. 2. Power curve and power coefficients of Gamesa G128 5MW wind turbine (up) and power matrix of Wave Star WEC (bottom).

3. Technical assessment of systems

The methods of characterizing energy variability and storage system sizing algorithm are introduced and proposed, and the technical assessment results are analysed and compared. It is known that energy storage systems (ESS) have been widely applied to reduce the intermittency of non-dispatchable renewables generations. In addition, the combined wind and wave energy conversion system has been proven to mitigate the energy variability of offshore energy farms. Therefore, the hybrid system involving WECs and WT can be considered as a 'virtual energy storage' system reducing the energy variability in the overall

system, which can provide a guide towards the smoothing effect of the HPU.

To assess the energy variability characteristics of the offshore energy farm and the size of the equivalent ESS, the following assumptions are made:

- Since the generation unit is not mounted on the same platform, the energy production profile of each generation unit/sub-unit is assumed to be identical. Therefore, the impacts from hydrodynamics and sediments of the sites on the downstream and/or downwind devices are disregarded in this paper.
- The equivalent ESS concept is utilized to define the energy supply consistency and generation variability reduction only. Other potential characteristic features of ESS are not considered in this paper, such as frequency control and voltage regulation.
- Although the round-trip efficiency (RTE) of ESS is not directly considered in the dynamic models, the 90th percentile of the accumulated state of charge (SoC) is used to estimate the ESS energy capacity and reflect the RTE impacts on the ESS size.

3.1. Characterization of energy variability

To compare WTESS and HPU, three statistical variability indexes are used to estimate the centred moving average filter (MAF) window size. Normalized average power variation (ΔP_m in per unit), large variation occurrence (Γ in %) and coefficient of variability (CV, dimensionless) are given by:

$$\Delta P_m = \frac{1}{N}\sum_{t=0}^{N}\frac{|P_t - P_{t-1}|}{P_{install}}, \tag{5}$$

$$\Gamma_N = A/N, A = \begin{cases} 1 & |P_t - P_{t-1}| > 0.1 \cdot P_{install} \\ 0 & \text{otherwise} \end{cases} \tag{6}$$

$$CV = \frac{\sigma_t}{\mu_t}. \tag{7}$$

where N is the number of sample data points and A is the number of power ramp events when the power difference exceeds 0.1 p.u. of total installed capacity. σ_t and μ_t are the standard deviation and mean value of power production time series. These variation indexes are used to evaluate the smooth effect of the HPU system and determine the MAF size to be able to define the size of the equivalent ESS in a WT.

In addition, the power ramping characteristics are investigated by using a swinging door algorithm proposed by the National Renewable Energy Laboratory (NREL) [10]. Three hours ramping window and 25% ramping rates are selected in this study. This is based on the previous studies which performed wind ramp events under hourly power generation data [62–64] and the details are given in Algorithm 1 in Appendix A.

3.2. Sizing equivalent energy storage system

Fig. 3 presents the principal framework of sizing the equivalent ESS in an offshore WT, which includes the evaluation of the multiple variability indexes to achieve the same level of variability characteristics as in the HPU system. Note that the major parameters in sizing include power capacity, P_{rated}^{ESS} in kW and energy capacity, E_{rated}^{ESS} in kWh.

The first step in sizing involves the MAF filter window size by the defined variability indexes (such as ΔP_m, Γ and CV) ensuring that the filtered power generation series achieve the equivalent variation characteristics as the HPU system. Then, the energy difference (deficit and surplus) can be obtained by comparing the WT generation data and MAF-filtered data. In the following step, the energy deficit and surplus are used to define the capacity of the ESS using the accumulated state of charge (SoC) method. Finally, to validate the estimated size, an ESS dynamic model is developed by using the SoC and Depth of Discharge (DoD). Furthermore, to avoid interannually variations, the

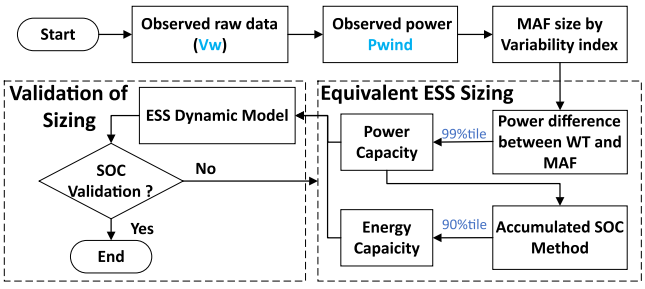

Fig. 3. Methodology developed for the equivalent EES sizing in WTs.

seven-year (from 2014 to 2020) WT generation data available about the site is used. This allowed to quickly estimate the size of the ESS by the given/target variation indexes and generation time series. Note that during this stage, the SoC and DoD are maintained within the technical limitations without overcharging/discharging and over-sizing the ESS. Note that the model developed here can be adapted to size the ESS in a renewable farm as well using the local demand and generation profiles [65].

The maximum charging/discharging rate (P_c and P_d) of the ESS are assumed to be equal to the rated power capacity of ESS (P_{rated}^{ESS}), which can be determined by the hourly power fluctuation (ΔP_t) given by:

$$\Delta P_t = P_t^{WT} - \mathrm{MAF}_t \tag{8}$$

where P_t^{WT} and MAF_t are the WT power generation time series and the MAF smoothed WT power time series. To statistically cover most power fluctuations, P_{rated}^{ESS} is defined by averaging the 99th percentile of ΔP_t each year from 2014 to 2020. The energy capacity is determined by the distribution of the accumulated SoC index, A_t, which is defined by:

$$S_t = \begin{cases} min(\Delta P_t, P_c) & \Delta P_t > 0 \\ max(\Delta P_t, P_d) & \text{Otherwise,} \end{cases} \tag{9}$$

$$A_t = \begin{cases} S_0 & t = 0 \\ A_{t-1} + S_t & \text{Otherwise} \end{cases} \tag{10}$$

where S_t is the charging or discharging power time series. Note that, as the initial values of S_0 present a significant impact on the accumulated data, the first step is to determine their initial values by $S_o^i = -mean(A_t^i)$ to balance the offset of SoC data series at each year i. Then, E_{rated}^{ESS} is estimated by taking an average of the 90th percentile of A_t^i at each year.

To validate the size and the SoC of ESS, the dynamics charging and discharging model of the ESS is proposed in this paper, given by:

$$\mathrm{SoC}_{t+1} = \mathrm{SoC}_t + \mathrm{NF}_t, \mathrm{NF}_t = \begin{cases} \mathrm{NF}_t^c & \Delta P_t \geq 0 \\ \mathrm{NF}_t^d & \Delta P_t < 0 \end{cases} \tag{11}$$

where SoC_t is the ESS state of charge and NF_t is the net power flow which is equal to NF_t^c in the charging model and equal to NF_t^d in the discharging model. The Eq. (12) and (13) aim to meet the constraints of SoC and converter ratings.

$$\mathrm{NF}_t^c = min\left[\Delta P_t, P_c, (E_{rated}^{ESS} - \mathrm{SoC}_t)\right], \tag{12}$$

$$\mathrm{NF}_t^d = -min\left[|\Delta P_t|, -P_d, \mathrm{SoC}_t\right]. \tag{13}$$

The power output (P_t^{out}) of WTESS and other constraints and assumptions are given by:

$$P_t^{out} = P_t^{WT} - \mathrm{NF}_t \tag{14}$$

$$E_{rated}^{ESS} \geq \mathrm{SoC}_i \geq 0, P_d < 0, P_c > 0, \mathrm{SoC}_0 = 0. \tag{15}$$

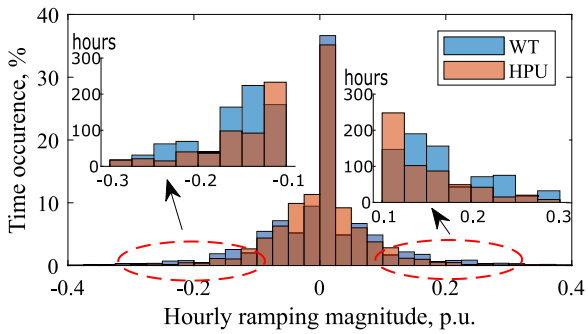

Fig. 4. Comparison of hourly ramping magnitudes between standalone WT and the HPU system.

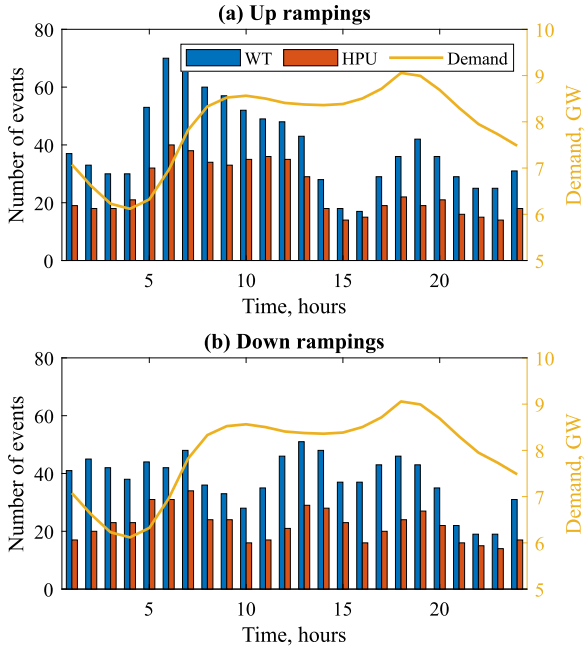

Fig. 5. Average daily up-ramp (top) and down-ramp events (bottom) with demand of Sydney in 2014.

3.3. Technical results

To demonstrate the method presented above for energy variability and storage sizing under different offshore energy farm configurations, the Sydney site was selected as the case study as it is one of the typical wind-wave sites in the world [43].

3.3.1. Energy variability and ramping

Fig. 4 shows the magnitude of hourly energy variation of standalone WT and the HPU system at the Sydney location in 2014. It can be seen in the figure, the standalone WT has a higher probability (hundreds of hours per year) of large energy variations (exceeding 0.1 p.u. of the installed power capacity) than the HPU system. In other words, the HPU system can significantly reduce ocean renewable energy intermittency. Note that, instead of 0.25 p.u. in ramping events detection, 0.1 p.u. is selected to investigate the energy variability in more detail.

To be able to analyse the ramping events, the daily up- and down-ramps events of the energy farm in Sydney location and the demand data of New South Wales (NSW) in 2014 are displayed in Fig. 5. In the figure, the yellow line represents the average daily demand. Generally, the HPU system significantly reduces both up- and down-ramping events across each hour of a day, by an average of 44.0% and 45.4% respectively. For example, it significantly mitigates (above 50%) the up-ramping during 2–6 AM (low demand period) and between 5–7 PM (demand up-ramp period). In addition, the occurrence of down-ramping in an HPU system reduces considerably (by 50%) from 8 AM to 12 PM and 4 to 6 PM. It is noted that some periods (e.g morning and evening) are sensitive to the power generation variations, resulting in a higher requirement for the firmness of renewable energy supply.

To investigate the seasonal energy dispatchability of both configurations, the ramp events in Sydney during four distinct seasons, Winter, Summer, Spring and Autumn, are studied and given in Fig. 6. It can be seen that the characteristics of ramping events vary among different seasons. In general, the HPU has the best performance in mitigating ramp events in Autumn. More specifically, during the winter season, the HPU system has a better energy smoothing effect (fewer up-ramps) in the morning (6 AM–10 AM) and the evening period (8 PM–11 PM), and particularly for the down-ramps events in the evening (3 PM–9 PM, during the peak demand period). In the summer season, the up-ramps of HPU system are significantly lower than the standalone WT (by 43%) during the morning period (2 AM–8 AM, see Fig. 6c), while limited benefits can be found between 9 AM and 4 PM (by a reduction of 2.5%). Conversely, down-ramps are reduced during the noon and afternoon (between 11 AM and 8 PM, see Fig. 6d) by 39.7% while a peak demand is also present. In the spring season, the number of daily up-ramps is only reduced by an average of 17% while a significant reduction can be found from 12 AM to 9 AM by up to 45% (see Fig. 6e). The down ramps reduction in the spring season is observed across the day by an average of 30%. In addition, during the autumn season, the HPU has the best mitigation on ramps events than other seasons. It is observed that both up- and down-ramps are significantly reduced across all day hours by an average of 55% and 51% compared to the standalone WT system. Moreover, the ramps events on two typical days are shown in Fig. B.1 in Appendix B for the reader's interest.

The statistics of the ramping event durations are given in Fig. 7. The results show that the period of the ramp events for both the WT and the HPU is about 3 h with above 50% of the total event occurrence, followed by the 4-hour ramping events. In addition, although the HPU increase the occurrence of the 3-hour ramping events, it significantly reduces the number of long-duration (greater than 3 h) ramping events. Note that the short periods of the ramps can be offset by an ESS (though not always), while those long periods of ramps events have a higher requirement on larger energy storage capacity. Moreover, the long-term energy intermittency of renewables usually requires expensive peak generation units (such as advanced gas and diesel power plants) to compensate for the shortage of supply, which significantly increases the electricity price in the spot market.

3.3.2. Storage sizing

Table 1 shows the ΔP_m, the Γ and CV of WT, WT with MAF and HPU under different window sizes. It can be seen that the MAF window size of 4 h for WT is selected as its variability characteristic are close to that of the HPU. The statistics of power rating and energy capacity in Sydney in 2014 are shown in Fig. 8. The power rating of ESS (P_{rated}^{ESS}) in 2014 is selected at 1223 kW as it covers the 99th percentiles of charging and discharging events. With regard to energy capacity (E_{rated}^{ESS} in kWh), 3502 kWh is used in 2014 by taking 90th percentiles of the energy capacity needed. Note that taking 99th percentiles is not the economical solution (requiring five times more energy capacity) due to significantly low events occurrence. In addition, the energy capacity is about three times the power rating. This is consistent with the most dominated ramping period (3 h). Furthermore, the average sizing results over seven years are considered to remove the impact of inter-annual size discrepancy. The final values of ESS power rating and energy capacity are estimated at 1100 kW and 3600 kWh.

To evaluate the equivalent size of ESS, the comparison of magnitude variations and the ramp characteristics of different system configurations are given in Appendix C. Both results validate the size of the

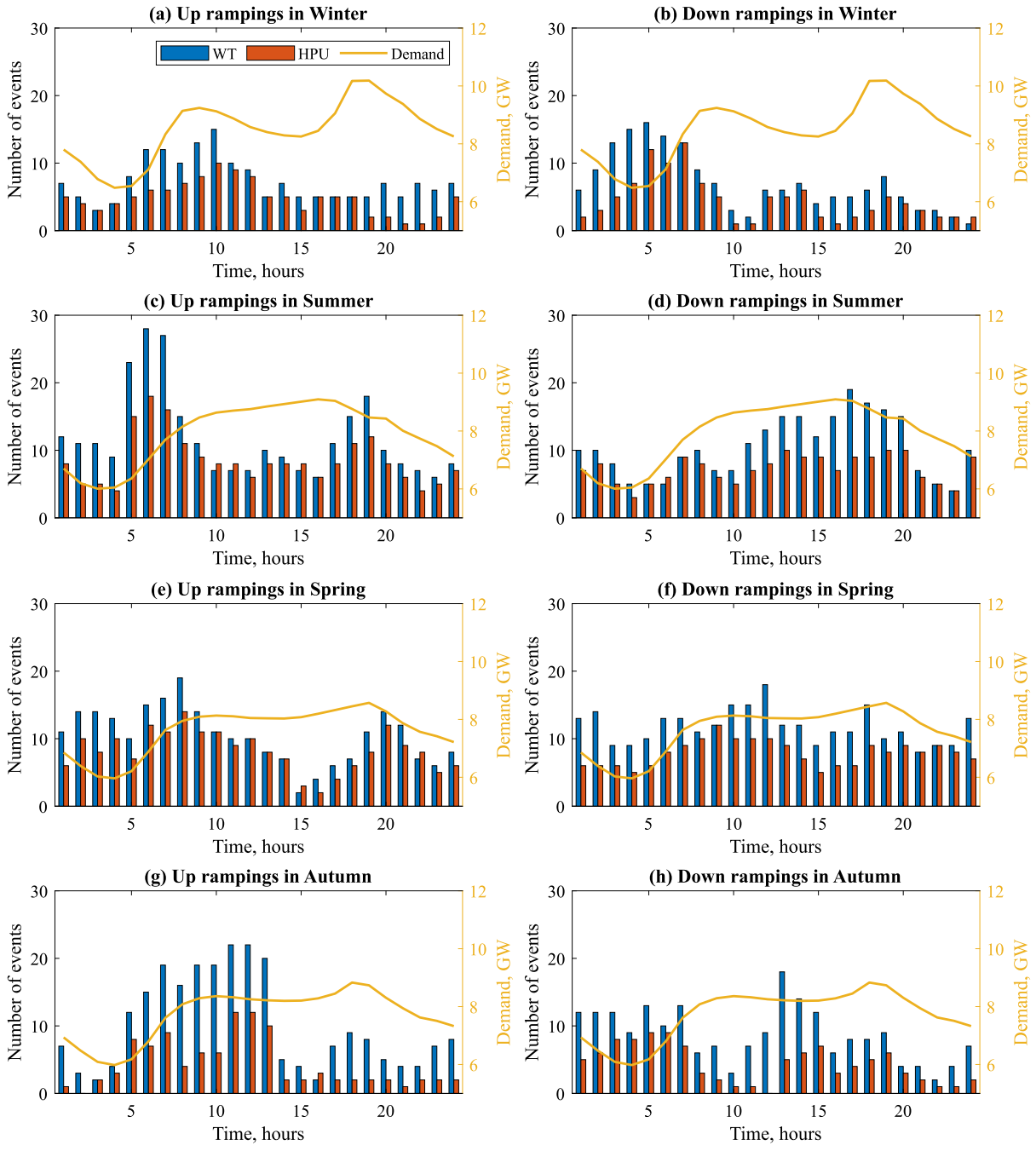

Fig. 6. Up- and down-ramp events in summer and winter for WT and HPU in Sydney location in 2014.

Table 1
Variation index for estimation of MAF window size in 2014.

Variability index	WT	MAF with various size (M)				HPU
		M = 2 h	M = 3 h	M = 4 h	M = 5 h	
ΔP_m	0.062	0.053	0.048	**0.044**	0.038	0.046
Γ(%)	19.7	17.4	14.0	**11.5**	8.9	14.0
CV	0.59	0.58	0.58	**0.56**	0.55	0.55

ESS for WT having the equivalent smoothing effect of the HPU system. Furthermore, the SoC of the designed ESS is analysed and the results show that the ESS is performed well within the allowable conditions (see Fig. C.3).

4. Economic assessment of systems

The combined wind and wave energy system and wind system with ESS are both proposed to be an effective solution to enhance the dispatchability of the ocean renewables in the future energy supply. Therefore, the lifecycle cost models of different system configurations (standalone WT, WTESS and the HPC) are developed here to provide a well-defined economic analysis for implementation in the future.

The economic assessments are conducted using a benchmark offshore farm with an installed capacity of 500 MW. The configurations of three offshore farms (WT, WTESS and the HPC) are summarized in Table 2. In this paper, a radial collector system is used as a benchmark farm layout (10 columns × 10 rows for WT and WTESS and 10 columns × 7 rows for HPU) since it is the simplest, shortest cable and it has been applied in the Horns Rev 2 wind energy farm owned by

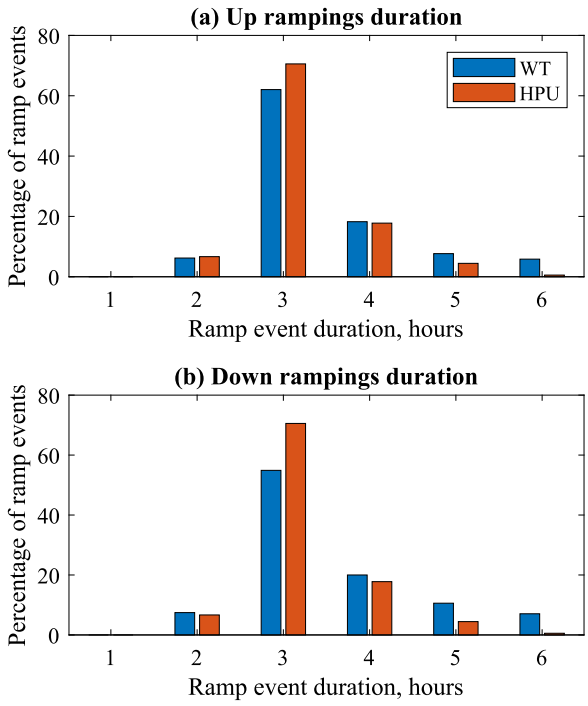

Fig. 7. Ramping duration in Sydney location in 2014.

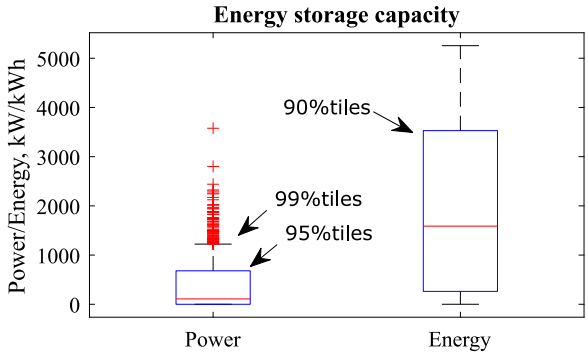

Fig. 8. Defining power and energy rating of energy storage.

Table 2
Three configurations of 500 MW exemplar energy farm.

Configurations	WT (5 MW)	WTESS (5 MW)	HPU (7.4 MW)
Unit number (N_i)	100	100	67
Total capacity (MW)	500	500	496
Project lifetime (years)	25	25	25
Interest rate r_{borrow} (%)	7.5	7.5	7.5
Farm availability (%)	94	94	96.3
Energy losses (%)	(1.8+7.7)	(1.8+7.7)	(1.8+7.7)

Orsted [66]. Based on the turbine size and general spacing requirement, the distance between each tower is about 7–8 turbine diameters (around 1 km) for the benchmark farm. Note that determining the optimal electrical cabling and layout of wind turbines may involve many trade-offs and is highly dependent on the location specifications [67,68]. Finally, the key economical results of a case study are given based on the sea site located 90 km east of Sydney.

To develop life-cycle cost model of proposed energy farms under various locations, certain assumptions are made:

- Firstly, using the current technology of the offshore tower foundations, different foundation types are considered for various water depths. For example, the bottom-fixed (jacket) and two different floating foundations (Tension-Leg-Platform and Hywind II) can be deployed in water depths below 35 m, 50–70 m and above 70 m, respectively.
- Secondly, the development and license of offshore energy farms vary significantly due to the feasibility of site selection, permitting and stakeholder engagements across the countries, which is disregarded in this paper and the proven cost estimation is selected for all locations.
- Other cost factors (such as labour cost, manufacturing cost, tax and subsidy) depending on local market maturity, supply chain and jurisdictional difference are not considered in this work, and the same approach is applied to all maritime areas.
- Finally, all the costs are converted to an average value in Euros (€) in 2022.

4.1. Life-cycle cost modelling

As it is given in Fig. 9, the life-cycle cost (LCC) of an offshore energy farm in this paper can be divided into two different subsystems costs: generation systems and connection systems costs (in yellow dashed box). Note that the generation systems involve the costs of subsystems under two scenarios: WT+ESS (in blue dashed box) and WT+WEC (known as HPU system in orange dashed box).

In terms of the project development procedure, LCC can be categorized by CAPEX (highlighted in cyan), OPEX (highlighted in green) and DCPEC (highlighted in grey). The bi-directional arrow-linked cost capsules represent the same cost model applied. The details of these cost capsules are described in the following subsections.

The levelized cost of energy (LCOE) is used to assess the economic potential of these different offshore energy farms, which is given by:

$$\text{LCOE} = \frac{\text{CRF} \cdot C_{invest} + \text{OPEX} + \text{CRF} \cdot C_{decom}}{\text{NAEP}}, \tag{16}$$

where C_{invest} is the overnight capital cost (CAPEX). OPEX and C_{decom} are the annual operational expenditure and the total decommission cost (DCAPEX). CRF is the capital recovery factor [69], which is defined by:

$$\text{CRF} = \frac{r_{\text{borrow}} \cdot (r_{\text{borrow}} + 1)^n}{(1 + r_{\text{borrow}})^n - 1}, \tag{17}$$

where r_{borrow} and n are the interest rate (7.5% p.a. used in this paper) and the number of annual payments to repay capital (25, the project economic lifetime). The Normalized Annual Energy Production (NAEP) from 2014 to 2020 is calculated by:

$$\text{NAEP} = \alpha \cdot \eta \cdot \left[\sum_{t=2014}^{2020} E_t \right] /7. \tag{18}$$

Here E_t is the energy generation at year t. α is the energy farm availability (percentage of time for normal generation of energy farm), depending on the window time for maintenance operations [70], and η is the energy conversion efficiency considering the total energy loss of the energy farm.

In this paper, based on the failure rates/events of different system categories (e.g. cable or foundations fails), the corresponding energy availability α for an offshore wind farm is estimated at 94% [71]. Moreover, 90.5% for overall energy efficiency is considered as a result of 1.8% of electrical losses and 7.7% of aerodynamics loss (farm weak effect) [72].

4.1.1. Capital expenditure

The CAPEX for an offshore energy farm can be represented by:

$$C_{invest} = C_{D\&C} + C_{Build} + C_{Install} + C_{Connection}, \tag{19}$$

$C_{D\&C}$ is the cost of development and consenting which includes but not limited to site selection, survey, characterization, permitting and array design. C_{build} and $C_{install}$ represents the building cost and installation

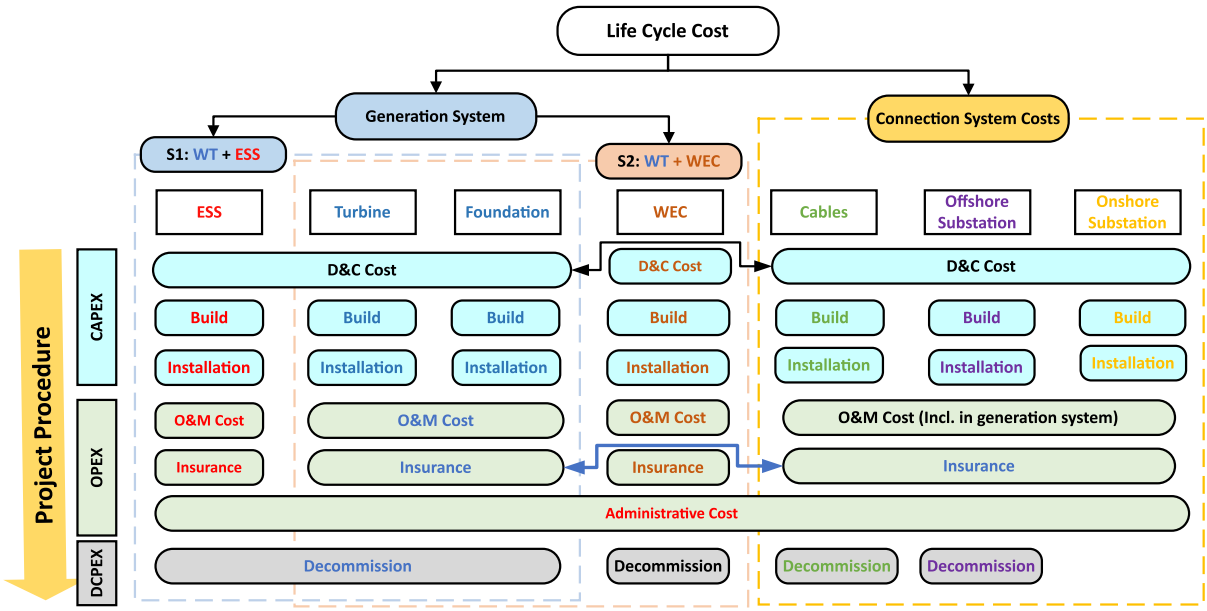

Fig. 9. The lifecycle cost diagram in an offshore energy farm: (1) by different subsystem cost modules, such as for generation systems and connection systems; (2) by different cost items during various project periods, such as CAPEX, OPEX and DCPEX.

cost of equipment. $C_{Connection}$ is the power connection cost for an offshore energy farm.

The D&C cost is one of the significant costs to the overall cost of an offshore energy farm. In this paper, the $C_{D\&C}$ of a 500 MW offshore wind farm is estimated at 105 M€, which is in line with the values of 105 M€ for an exemplar 500 MW offshore wind farm in the studies [44,71] and the value of 210 k€/MW in the study [73]. In addition, due to the lack of wave projects being commercialized, the $C_{D\&C}$ for a WEC array is estimated by 12% of the total initial investment of WEC farm [74,75].

The building cost of the fully-equipped devices, such as the turbine cost ($C_{turbine}$) and the foundation cost ($C_{foundation}$), the ESS cost (C_{build}^{ESS}) and the WEC device cost (C_{build}^{WEC}), are given by:

$$C_{build}^{WT} = C_{turbine} + C_{foundation}, \tag{20}$$

$$C_{build}^{ESS} = \mathrm{UCE}_{ESS} \cdot E_{rated}^{ESS} + \mathrm{UCP}_{ESS} \cdot P_{rated}^{ESS}, \tag{21}$$

$$C_{build}^{WEC} = \mathrm{UC}_{build}^{WEC} \cdot P_{rated}^{WEC}, \tag{22}$$

where, UCE_{ESS} and UCP_{ESS} are the unit cost of power (€/kW) and energy capacity (€/kWh) of the ESS respectively. P_{rated}^{WEC} and $\mathrm{UC}_{build}^{WEC}$ are the rated power and the unit cost of a WEC system, respectively. Note that 3100 €/kW is used in this paper for a utility-scale of wave energy farm [76].

The turbine cost $C_{turbine}$ usually can be estimated by a function of the turbine capacity [77,78]. Within the context of this paper, the turbine cost is estimated by Eq. (23).

$$C_{turbine} = 2.95 \cdot 10^3 \cdot ln(P_{rated}^{WT}) - 375.2 \text{ [k€]/turbine} \tag{23}$$

The foundation cost relies on the platform types significantly which are determined by the water depth and the wave conditions in the deployed locations. In this work, the bottom-fixed foundation is selected in a location with a water depth lower than 35 m and its cost, $C_{foundation}$, can be estimated by a parametric expression reference to the hub height (h), turbine diameter (D) and water depth (d) [77,79].

$$C_{foundation} = 320 \cdot P_{WT}\,[1 + 0.02(d-8)] \cdot \left[1 + 0.8 \cdot 10^{-6}\left(h(\frac{D}{2})^2 - 10^5\right)\right] \text{ [k€/turbine]} \tag{24}$$

Table 3
Substation cost for a 500 MW offshore energy farm.

Types	Construction	Installation
Offshore Substation	72 M€ (60 M£ [77,81])	21 M€ (17.5 M£ [82])
Onshore Substation	18 M€ (15 M£ [77])	15 M€

The floating structures, such as Hywind II (estimated cost at 3.74 M€ per turbine) and Tension-Leg-Platform (TLB X3, estimated cost at 1.20 M€ per turbine), are selected for the locations with water depth of 40–70 m and above 70 m, respectively [71].

The installation cost ($C_{install}$) varies under different WTs and foundations [72]. In this case, the installation cost for 5 MW WT is estimated by Eq. (25) [79].

$$C_{install}^{WT} = 0.1 \cdot C_{turbine} + 0.5 \cdot C_{foundation}. \tag{25}$$

The resulted cost of WT installation (1675k€) in this paper is within the values of 1538 k€ and 1951 k€ of monopile type and jacket type respectively [71]. Regarding the WEC installation cost, it is normally estimated at 8%–17% of the initial investment. Thus, the WEC installation cost in this paper is estimated at 13% [76,80] of initial WEC investment of about 1.16 M€.

The costs of power connection to the grid ($C_{Connection}$) include the substation cost (C_{sub}, generally required when installed power above 100 MW or far from shore) and cable costs, which are calculated by:

$$C_{Connection} = C_{subs} + \sum_{a=1}^{3} \mathrm{UC}_{cable}^{a} \cdot L_a, \tag{26}$$

The substation costs (C_{subs}, including the onshore and offshore substation) of a 500 MW offshore energy farm are estimated by Table 3.

In the second term of Eq. (26), a denotes the cable type: $a = 1$ for the inter-array cable between WT and WEC; $a = 2$ for medium voltage (MV) array cable; $a = 3$ for high voltage transmission cable. UC_{cable}^{a} and L_a represent the unit price (k€/kM) and length (in km) of the cable type a. Note that, for simplicity, the L_1 equals to the distance between WT and WEC; L_2 is estimated by a linear regression equation ($R^2 = 0.956$) with two parameters of device number (N_i) and its diameter (D) [77]. L_3 are assumed to be equal to the distance to shore (90 km).

$$L_2 = 1.125 \cdot N_i + 1.055 \cdot D - 122.64 \text{ [km]}, \tag{27}$$

Table 4
Acquisition cost of cables for a 500 MW farm [71,72,77].

Cable types	Specification	Acquisition	Installation
UC^1_{cable}	33 kV, 150 mm^2	213 k€/km	189 k€/km
UC^2_{cable}	33 kV, 300 mm^2	225 k€/km	189 k€/km
UC^3_{cable}	320 kV, 1500 mm^2	443 k€/km	590 k€/km

The HVDC technology is applied to transmission cable in this paper and due to the lack of the medium voltage level of DC cable cost data, the DC inter-array cable cost is estimated by the cost ratio between HVAC and HVDC cables. Their cost details are summarized in Table 4.

Due to the limited knowledge of decommissioning of the offshore wind farm, this cost is estimated in relation to the installation cost with ratios of 70%, 90% and 10% for the completed wind turbine (incl. foundations), substations and undersea cables, respectively [83]. Therefore, the total cost of decommissioning in this case study is about 512 k€/MW (2.69 M€ per turbine), which is within the range of 200k–600k €/MW [84] and is slightly higher than the data (503 k€/MW) in study [85].

4.1.2. Operational expenditure

The annual operational expenditure comprises the operation and maintenance cost ($C_{O\&M}$), insurance cost ($C_{insurance}$) and administrative cost (C_{admin}), given by:

$$\text{OPEX} = C_{O\&M} + C_{Insurance} + C_{admin}, \tag{28}$$

where $C_{O\&M}$ includes the O&M cost of WT ($C^{WT}_{O\&M}$), WEC ($C^{WEC}_{O\&M}$) and ESS ($C^{ESS}_{O\&M}$).

In [44], $C^{WT}_{O\&M}$ is calculated based on the WT rated power capacity, about 133 €/kW. The $C^{WEC}_{O\&M}$ is estimated to be 4% of annual CAPEX of WEC [76]. The O&M cost of ESS $C^{ESS}_{O\&M}$ depends on its power capacity and energy throughput, which is given in the following section.

The insurance costs ($C_{insurance}$) rely on the development phase of the project and different calculation methods are proposed in previous literature, such as 15% of O&M cost in [70], 15 to 20 €/kW [71] and about 1% of the initial cost of WT [86]. In this study, the unit insurance cost of 19 €/kW/year is used for the selected WT. The insurance cost of ESS is estimated by 15% of its O&M cost or 0.48% of total cost [87]. Thus, the average value is used in this work, given by:

$$C^{ESS}_{insurance} = \left(0.15 \cdot C^{ESS}_{O\&M} + 0.48\% \cdot C^{ESS}_{build}\right)/2. \tag{29}$$

The insurance cost of a WEC is estimated as 2% of the O&M cost of co-located farm [44]. Furthermore, the fixed annual labour (such as technician and managers services) and administrative cost (C_{admin}) is estimated at 4.77 M€ in this study based on the 500 MW benchmark wind farm [71].

4.1.3. Validations of the cost modelling

Due to the commercial sensitivity (which is not readily available) and the limited data available about various components (such as the utility-scale of wave energy farms and the decommissioning cost of an offshore wind farm) of offshore farms, it is difficult to confidently estimate the detailed cost model. In addition, the accurate cost also relies on specific characteristics of the farm, including location characteristics, technology cost and associated market or supply chain. Therefore, in the analysis, the validations of the major cost parameters of offshore energy farms are considered.

In general, the CAPEX (incl. decommissioning cost) of offshore wind is estimated at €/kW in this paper which is comparable with the recent value of 3029 €/kW (4430 AUD/kW by [88]) and 3388 €/kW (3185 USD/kW by [17]). The annual OPEX of offshore wind is estimated at 158 €/kW per year which is higher than the values of 135 €/kW (113 £/kW per year [89]) and the value of 145 €/kW (149.9 USD/kW in [88]). This is due to the far shore sea locations than the most existing offshore wind farms. Regarding the HVDC transmission cost (covering the cables and substations), its normalized value is estimated at €/MW/km (7710 AUD/MW/km). Note that this is close to the normalized values of 7600 AUD/MW/km in the MarinusLink HVDC project [90] and 6100 AUD/MW/km in the Basslink HVDC transmission project [91] in Australia. In addition, the total cabling cost in this paper is estimated at 2898 €/MW/km which is 14% lower than 3373 €/MW/km (2833 £/MW/km) given in [81].

Table 5
Cost parameters of various BESS [65,92].

BESS	UCP_{ESS}	UCE_{ESS}	Fixed cost & Variable cost		Life years
	(€/kW)	(€/kWh)	(€/kW-yr)	(€/kWh-yr)	Avg.
Li-ion	388	372	10	0.0003	12.5
Redox flow	450	745	16	0.0003	20
Lead–acid	460	436	11	0.0003	5
Sodium sulphur	450	794	70	Included in fixed cost	15

4.2. Scenario definitions

4.2.1. Scenario 1: Wind turbine with energy storage system

The lifecycle cost models of Scenario 1 (S1: WTESS) that integrate WT with an equivalent size of the ESS are analysed first. It is assumed that the application of ESS has a limited impact on the existing WT technologies and the deployment of an offshore wind farm. Therefore, some cost items of the stand-alone wind farm S1 remain as they are, such as the D&C cost ($C_{D\&C}$), connection cost ($C^{S1}_{Connection}$) and administrative cost (C_{admin}). The build cost in S1 includes the WT cost (C^{WT}_{build}) and ESS cost (C^{ESS}_{build}, including its installation cost).

In terms of ESS, different mechanical energy storage systems (MES) are investigated for marine energy farms, such as the flywheel and gas accumulators in a WEC system [11] and the compressed air energy storage in the offshore wind turbine [13]. This paper considers the battery energy storage system (BESS) due to the modularized design, high power/energy density, smaller size and flexible control scheme compared to the MES.

The technical applicability and economic feasibility of various BESS for offshore energy farms in light of the energy dispatchability to local demand are investigated in [65]. The comparisons of different BESS are discussed in Appendix C. The Li-ion batteries are selected due to their better overall performance in terms of technical and economic feasibility [65]. In this paper, its average lifetime is assumed at 12.5 years and the replacement cost of the storage unit (excluding the power unit, see in Fig. 1c) is included in the case study. The economic parameters of BESSs are shown in Table 5. Note that the currency exchange rate between USD and EURO in this table is estimated at one in the average of 2022.

The O&M cost of BESS can be divided by the fixed cost and variable cost. The fixed cost (unit in €/kW-yr) includes all necessary maintenance and operation expenses during its economic lifetime and is unrelated to the energy usage. The variable cost (unit in €/kWh-yr) considers all costs necessary to the wear and tear of the storage system during its lifetime operation. Therefore, it is based on the annually charging and discharging energy throughput. Both costs can be estimated by the normalized value given in Table 5. Lastly, the insurance cost in S1 is estimated to be 2% of $C^{S1}_{O\&M}$.

4.2.2. Scenario 2: Hybrid power unit

The lifecycle cost models of the HPU system in Scenario 2 that accommodates one 5 MW WT with four 600 kW WECs are analysed in this section. Although, the costs of the D&C, equipment and the installation of the HPU system will be shared due to coordinated efforts, these costs are considered separately in this paper. Note that the total installation cost of WT and WEC is estimated to be reduced by 10% due to sharing the shipping vessel, storing and labour costs [70].

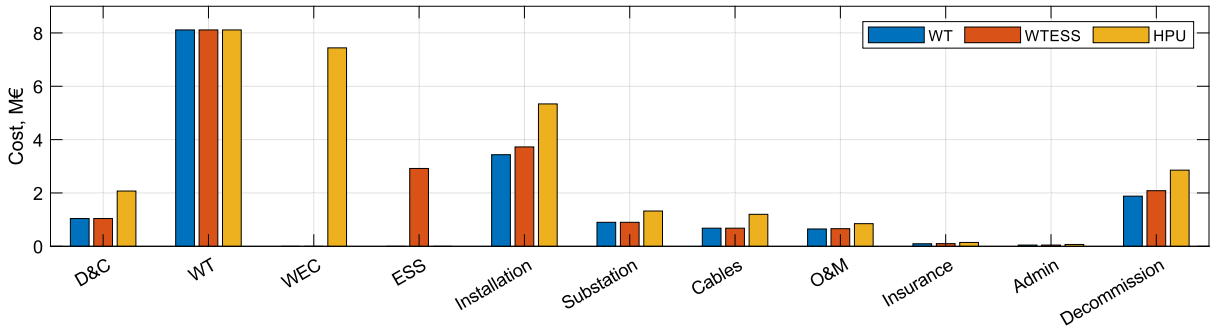

Fig. 10. Cost breakdown of one power generation unit under three system configurations.

Since the co-located energy farm with the same installed capacity, the costs of on-/off-shore substations and export transmission cables remain constant. In contrast, the inter-array cables should be adjusted resulting from the different energy farm configurations, such as the consideration of cabling between WT and WECs. The costs are given by:

$$C^{S2}_{inter-array} = \mathrm{UC}^{2}_{cable} \cdot L^{S2}_{2}(N_3, D), \tag{30}$$

$$C_{WEC-WT} = 4 \cdot \mathrm{UC}^{1}_{cable} \cdot L_1 \cdot 1.4, \tag{31}$$

Here, N_3 is the number of HPU in a 500 MW energy farm. C_{WEC-WT} represents the cable cost between WT with four WECs, and its length is equal to 1.4 times of distance between WEC and WT (L_1) due to the slack of the cables [71].

Due to the common synergies in maintenance and service tasks, the O&M cost achieves a reduction of about 12% [70]. The administrative cost is assumed the same as in the standalone WT farm. More importantly, since the WEC array somehow provides shelter for the energy farm, the accessibility for maintenance tasks is estimated to be increased. Therefore, the energy availability (η) of the combined energy farm is improved by 2.3% [70] at 96.3%.

4.3. Economic results

The total cost breakdown of three system configurations in the Sydney site is shown in Fig. 10. It can be seen that the WT acquisition cost, such as the turbine and the floating foundations (exclude installation), are the most costly items among the others, about 10 M€. This is in line with the most lifecycle cost studies reported in [71,77,81,85]. Due to the immaturity of the wave energy technology, WEC devices cost in an HPU accounts for about 90% of the WT cost while its capacity (2.4 MW) is only 48% of WT capacity (5 MW). However, WEC cost is predicted to be significantly reduced in the future as more mature and advanced technologies become available as reported in [93]. In light of the long transmission distance and the deep water conditions, the total installation cost, covering the turbine, foundations, WEC and all cables, is the second highest cost component.

Although the power unit number (Ni) is reduced from 100 to 67 (by 33%), the expenses of installation and cable in the HPU system are higher than the standalone WT and WTESS by about 34%. This introduces an extra cost due to WEC-WT cables and customized-built installation vessels and transportation equipment. Moreover, EES cost is also significant compared to other factors due to the relatively high cost of BESS. In addition, the substation costs allocated to each HPU are higher than that of WT and WTESS systems. This is due to the fact that, with the given fixed total installed capacity of offshore energy farms, the number of units is reduced. Therefore, the shared substation cost is increased accordingly. The detailed cost breakdown of three offshore energy farm configurations is summarized in Appendix D.

Table 6 summarizes the annual energy production, LCOE and the ramp statistics of three system configurations. It is clear that the WT-only energy farm has the lowest LCOE at the value of 99.6 €/MWh while it exhibits the highest ramping events occurrence at the value of 21.2% in a year. Although WTESS significantly reduces the ramp occurrence from 21.2% to 13.3%, it presents the highest LCOE cost at the value of 115.9 €/MWh. The HPU present the advantages of not only the best reduction of ramp occurrence but also having 8% lower LCOE than WTESS at the value of 107.9 €/MWh due to approximately 48% more energy production than the other two systems. In addition, since the cost of the stand-alone WEC system is outside the scope of this paper, its LCOE is obtained from other studies, which is significantly higher, above 300 €/MWh as reported in [28,29,94].

Table 6
Energy production, LCOE and ramp statistics of three system configurations in Sydney location.

Configurations	WT	WTESS	HPU	WEC^{*}
Production (GWh/yr):	26.0	26.0	38.6	12.6
LCOE (€/MWh):	99.6	115.9	107.9	>300
Ramp Occurrence (%):	21.2	13.3	12.7	10.4

5. Discussion

It is known that the wave source characteristics and the location specifications are two key factors impacting the assessment of an offshore energy farm as well as their associated cost, specifically when WEC is deployed in a combined energy farm. The sensitivities of techno-economic feasibility of three system configurations to these two factors are discussed, which provide comprehensive insights and understanding of deploying future offshore combined energy farms.

As it was stated previously, multiple locations across the world (three locations in Australia, one location in Europe and one location in the US) are selected to cover the diversity of wave system types in the World. Therefore, it can be assumed that the analysis and methods presented here are also applicable to evaluate other sea locations.

5.1. Resources sensitivity analysis and integrated assessment

Given the knowledge of wave generation and propagation, the ocean waves can be categorized into three types: wind-wave, swell wave and mix-waves (mixed of the first two types). The wind-waves are generated locally and present a strong correlation with the local wind. In contrast, the swell waves are propagated from thousands of miles away and weakly coupled with the local wind field as it obtains enough energy to travel beyond their generation area or fetch. The mixed-waves combine both wind-wave and swell waves. Since the interaction between wind and wave resources is critical for the development of a combined energy farm [43], multiple locations with various wave types are investigated in this paper as summarized in Table 7.

Due to the varying water depths in different sea locations, different foundation types are also selected. For example, the bottom-fixed foundation (Jacket type) is selected for a 5 MW WT at 35 m water depth in

Table 7
Energy variability and economic comparison at multiple locations with various characteristics waves.

Wave types (Location)	Distance, Depth (km, m)	Foundation types	C_r/τ (-/h)	P_{wind}&P_{wave} (kW/m^2, kW/m)	Systems	ESS (kW/kWh)	CV	Mean Var. $\overline{\Delta P_m}$	Ramp events (%)	DT (%)	Production (GWh/yr)	LCOE (€/MWh)
Wind-wave (Sydney, AU)	90 km, ≥100 m	Hywind (Floating)	0.60/5	1.02/21.6	WT	–	0.59	0.20	21.2	8.0	26.0	**99.6**
					WTESS	1100/3600	0.57	**0.15**	13.3	6.5	26.0	115.9
					HPU	–	**0.47**	0.17	**12.7**	**0.6**	**38.6**	107.9
Mixed wave (Port Lincoln, AU)	10 km, ~70 m	Hywind (Floating)	0.41/14	0.65/53.7	WT	–	0.75	0.18	15.6	11.9	20.4	**122.9**
					WTESS	900/3000	0.73	**0.14**	12.0	10.6	20.4	140.0
					HPU	–	**0.48**	0.16	**8.4**	**0.6**	**32.7**	123.2
Swell wave (Cliff Head, AU)	20 km, ~50 m	TLB X3 (Floating)	0.21/4	0.49/39.3	WT	–	0.72	0.20	26.1	12.1	19.6	**103.4**
					WTESS	1000/3800	0.69	**0.15**	19.5	10.0	19.6	125.4
					HPU	–	**0.50**	0.17	**15.5**	**0.5**	**31.8**	116.0
Strong wind-wave (North Sea, EUR)	8 km, ~35 m	Jacket (Bottom-fixed)	0.81/1	0.87/13.3	WT	–	0.65	0.18	21.7	10.6	24.4	**97.1**
					WTESS	450/1120	0.64	**0.15**	22.3	10.2	24.4	102.8
					HPU	–	**0.64**	0.16	**12.4**	**6.6**	**33.6**	116.2
Mixed wave (Blunt Reef, USA)	10.5 km, ~80 m	Hywind (Floating)	0.31/6	0.64/35.8	WT	–	0.79	0.17	8.5	20.5	20.9	118.7
					WTESS	750/2600	0.78	0.16	7.7	20.1	20.9	133.0
					HPU	–	**0.56**	0.16	**5.1**	**0.87**	**34.5**	**116.5**

the North Sea location. In addition, $\overline{\Delta P_m}$ is defined by the mean value of hourly energy variations larger than 0.1 p.u. of the installed capacity. The downtime (DT) in Table 7 is considered as the percentage of hours that total energy production is below 0.05 p.u. of installed capacity. In this paper, the resources characteristics (such as wave types, correlation C_r and lag time $\tau(h)$), location specifications (such as water depth and distance to the shore), energy storage capacities, energy variation indexes (such as CV, mean value of significant variations, ramp events occurrence), energy availability (such as generation downtime and annual production) and LCOE, are all given in Table 7.

Overall, the HPU systems (except the case in the North Sea) present the most significant energy variation reduction and the lower value of LCOE compared to WT with ESS configurations. Due to the long transmission distance and deeper water, the energy farm deployed in the Sydney location has the highest cost of equipment (such as turbine with the platform, ESS and WEC) and installation. However, its LCOE presents relatively low values among all three system configurations due to the highest wind energy availability (1.02 kW/m^2) than other locations, with an annual production of 26.0 GWh for wind and 38.6 GWh for an HPU.

Since the different floating platform types are deployed, the LCOEs of all three system configurations are significantly different between Port Lincoln and Cliff Head, although they have similar energy production per year. Note that when considering the expensive foundation for offshore WT, the HPU system presents better cost reduction than the WT with an equivalent ESS. For example, the cost reduction is 14% (140 versus 123.2 €/MWh) and 8% (125.4 versus 116.0 €/MWh) in Port Lincoln (by Hywind) and Cliff Head (by TLB X3), respectively.

In addition, Port Lincoln has a lower CV and ramping occurrence, which can offer more firm power generation capacity similar to the conventional dispatchable power system. It is noted that the North Sea presents a strong correspondence (with the highest correlation of 0.81 and the shortest lag time of 1 h) between wind and wave resulting in the smallest size of equivalent ESS. This indicates the poorest performance of power variations reduction, which also can be identified by the comparison of CV between WT and HPU. However, due to the short transmission distance, shallow water and strong wind source, the North Sea has the lowest LCOE for offshore wind and WTESS at 97.1 €/MWh and 102.8 €/MWh, while the HPU does not have economic competitiveness with a LCOE of 116.2 €/MWh. The potential reasons are the low wave resource and poor smooth effect of the combined system.

The LCOE of HPU in the Blunt Reef location is found lower than that of the WT farm (116.5 versus 118.7 €/MWh) and is 12.4% lower than that of the WT with ESS energy system (133 €/MWh). Note that under the similar geographical specifications (water depth and distances) between Port Lincoln and Blunt Reef, Port Lincoln has better resource availabilities compared to the Blunt Reef (especially for wave power density, 53.7 versus 35.8 kW/m), while it generates less energy production annually. This is due to the fact that the power ratings of WECs in Port Lincoln have been relatively underestimated.

5.2. Energy variability mitigation

The values of various energy variation indexes of the HPU configuration are reduced by different degrees in all locations (except the North Sea). It is important to note that the combined system can significantly reduce both CV and DT indexes while the application of BESS cannot. The possible reason is that the BESS applied in WT is not desired for addressing the relative long-term energy variations (a few days to seasonal) in wind resources. However, the combined system can offset these issues by the complementary characteristics between wind and wave (such as low correlation and long lag time) [43]. In addition, the ESS cannot significantly mitigate the large intermittency from wind resource falls, which is consistent with the results of downtime given in Table 7. Conversely, the BESS presents better performance on the mean value of major power variations ($\overline{\Delta P_m}$) as it is the magnitudes of short-term variation. Furthermore, it is found that although the BESS can reduce the occurrence of the ramping event, it has less impact on reducing the number of larger ramp events in Port Lincoln and Cliff Head with high CV. This explains the fact that the MAF result can match the small-to-medium ramping characteristics (between 0.1 p.u.to 0.25 p.u see in Fig. C.1) of the HPU, while statistical differences between the ramp events appear in Table 7 due to the unmatched large ramping events (≥0.25 p.u.). This also indicates that the ESS (BESS in this case) is not a practical solution to offset the significant and long-term intermittency of wind energy, which in turn indicates the unique advantage of the HPU on the medium-to-long term of energy shortage.

Typically, the long-term (one to a few hours) duration of renewable energy deficit requires the final unit generation capacity in the grid to compensate the imbalance between the supply and the demand. This is known as Capacity Credits (CC) which defines the capability of conventional generators that can be replaced by renewable energy systems and/or the ESS [95]. The coordinated wind-hydro energy system [96] and the Solar PV system coordinated with battery system [97] can increase the CC. Although the CC study is not the focus of this paper, due to the energy variability reductions achieved in the HPU, it can be concluded that the combined energy system can increase the CC.

It has to be emphasized that the primary aim of BESS used in a WT is to reduce the energy variability to achieve the same level of variability as the HPU system. However, in practice, the size of ESS for WT depends on a number of factors, such as the correlations, power potential and energy variability between the wind and the wave resources. Therefore, it is hard to quantify the explicit trade-off between these

factors. However, it can be concluded that the costly ESS may not be the sole option for reducing offshore energy intermittency. Furthermore, the weight and volume of ESS significantly impact the dynamics and stability of the common platform, especially in the floating foundations. Therefore, minimizing the marine ESS size is desired and necessary for future commercialization. However, it is also recognized that the BESS arrangement can offer a fast response to power intermittency that is not available in other storage options. In addition, the virtual energy storage concept for WEC in a combined system can be adapted via advanced WEC control to achieve more unique functionalities, such as power regulation, frequency control and participation in the local electricity market, which is sensitive to dispatchability and response to the ramping events. For example, via advanced control strategies, the WEC are more actively generating power based on the WT generation pattern, to compensate for power generation when the wind is low while wave energy is available.

6. Conclusion

This paper investigates three offshore renewable energy conversion systems: stand-along WT, WT with ESS and the HPU system, in terms of their energy variability, energy storage requirement and lifecycle cost. The ramping characteristics of offshore renewables are studied by using a case study associated with local demands. A novel equivalent energy storage concept is proposed and developed to qualitatively and quantitatively the energy smoothing performance of various system configurations. In addition, high-fidelity economic models are developed to assess the economic feasibility of each conversion system with consideration of energy variation properties. Moreover, the sensitivity of system configurations to wind and wave characteristics is investigated in different potential sea sites.

The technical assessment results indicate that the HPU has the unique capability to form more dispatchable and predictable ocean renewables generation for providing a consistent and firm electrical supply. More specifically, the HPU system can effectively reduce power ramp events by up to 50% compared to the standalone WT system. However, these properties vary in seasonal and locations and highly depend on the surgeries between wind and wave resources, such as densities and correlations. In addition, the HPU system has great potential to prevent a significant and long-term shortage of wind energy supply which conventional battery storage systems cannot address effectively. Note that the discrepancies of the equivalent ESS sizes reflect the performance of the energy smooth by the HPU system at different offshore sites.

The economic analysis shows that a highly competitive cost can be offered by the HPU among different wave types at various locations. The value of LCOE for the HPU system is lower than that for the WT system with equivalent ESS by up to about 15% in most studied locations (except for the North Sea). It indicates that, given the similar energy dispatchability, the HPU system presents better cost competitiveness. However, these benefits vary in different locations.

There are two limitations in this study. Firstly, due to the lack of convergence towards a mature WEC and significant cost uncertainties involved in BESS, the economic performance of the combined energy system and ESS is hard to predict and estimate accurately. Secondly, the power generations of WT and WEC are estimated by assuming negligible interactions between devices. Future research work will study the sensitivity of economic models for hybrid power units and investigate the techno-economic feasibility of various ESS types applicable to offshore renewable farms.

CRediT authorship contribution statement

Qiang Gao: Conceptualization, Methodology, Analysis, Validation, Writing – original draft. **Rui Yuan:** Methodology, Analysis, Validation, Writing – original draft. **Nesimi Ertugrul:** Supervision, Knowledge, Writing – review & editing. **Boyin Ding:** Supervision, Knowledge, Analysis, Writing – review & editing. **Jennifer A. Hayward:** Knowledge, Analysis, Validation, Writing – review & editing. **Ye Li:** Knowledge, Analysis, Writing – review & editing.

Declaration of competing interest

The authors declare that they have no known competing financial interests or personal relationships that could have appeared to influence the work reported in this paper.

Data availability

Data will be made available on request.

Acknowledgements

The authors acknowledge the Australia–China Science and Research Fund and Australia–China Joint Research Centre of Offshore Wind and Wave Energy Harnessing funded jointly by the Australian Department of Industry, Science and Resources (ACSRF66211) and the Ministry of Science and Technology of China (2017YFE0132000).

Appendix A. Algorithm of ramping detection

The research on power ramp events was first proposed in 2007 [98]. The most versatile and widely used method for ramping detection is a swinging door algorithm (SDA) proposed by the National Renewable Energy Laboratory (NREL) [10] as shown in Algorithm 1. There are two essential parameters in the SDA-based methods, namely ramping window and ramping rates which are 3 h and 25% in this paper [62]. To clarify the ramp events in this paper, the relevant definitions are given as follows: (1) *Ramp events*: A ramp event is considered to occur when the change of power time series P_t (increase or decrease) in a given time interval Δt is larger than a predefined threshold value Θ, i.e., $|P_{t+\Delta t} - P_t| \geq \Theta$; (2) *Up ramping*: Given a ramp event whose change of power is positive, i.e., $P_{t+\Delta t} - P_t \geq \Theta_u > 0$; (3) *Down ramping*: Given a ramp event whose change of power is negative, i.e., $P(t+\Delta t) - P(t) \leq \Theta_d < 0$.

Algorithm 1 Swinging Door Algorithm

Require: P_t: power generation time series with the length of N, S: swing door size; Θ_u: up ramping events, Θ_d: down ramping events, Y: ramping event labels

$P_{max} \leftarrow max(P_t)$ ▷ generation capacity
$\kappa \leftarrow N - S$ ▷ count sliding steps
$Y^u, Y^d \leftarrow [0, 0, \dots 0]$ ▷ initialise ramp labels
for $i = 1, 2 \dots \kappa$ **do**
  for $j = 1, 2 \dots S$ **do**
    if $P_j - P_i > P_{max} \times \Theta_u$ **then** ▷ up ramping
      $Y^u_{[i:i+j]} \leftarrow 1$ ▷ assign 1 to up ramp labels
      break
    end if
    if $P_i - P_j > P_{max} \times \Theta_d$ **then** ▷ down ramping
      $Y^d_{[i:i+j]} \leftarrow 1$ ▷ assign 1 to down ramp labels
      break
    end if
  end for
end for
return Y^u, Y^d.

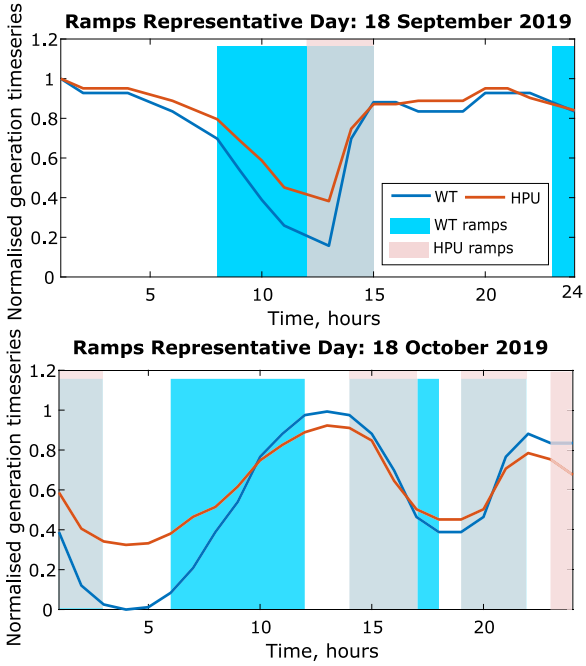

Fig. B.1. Ramps of standalone WT and the HPU system on two typical days.

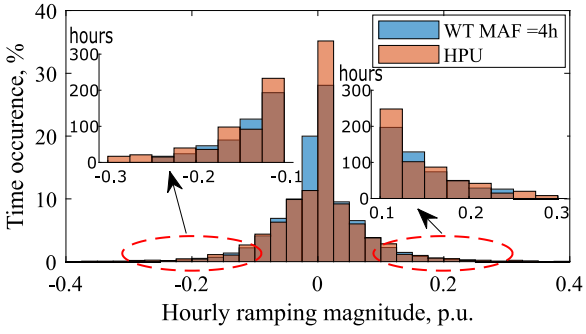

Fig. C.1. Histogram of hourly power ramping.

Appendix B. Ramps events in typical days

Fig. B.1 shows the power ramp events of the standalone WT and the HPU system in two representative days in the Sydney location. It can be seen that, due to significant wind speed changes, both up- and down-ramp events are detected for a wind-only system between 8 AM and 3 PM on 18 September 2019. Differently, the HPU system eliminates the up-ramp events between 8 AM and 12 PM on the same day and reduces the ramp events duration, probably because of the continuing supply of wave energy during the same time. Similar characteristics can be found on the day of 18 October 2020. The up-ramps only appear in the standalone wind system from 6 AM to 12 PM, whereas no such events for the HPU system. However, it is noted that due to the reduction in wave energy source, a down-ramps event is found for the HPU system, which does not appear in the standalone system.

Appendix C. ESS sizing results and comparison

To validate the equivalent size of ESS, the magnitude of histogram variations between the WT with MAF (4 h) and the HPU system are compared in Fig. C.1 and their results indicate an appropriate estimation of MAF window size compared to Fig. 4.

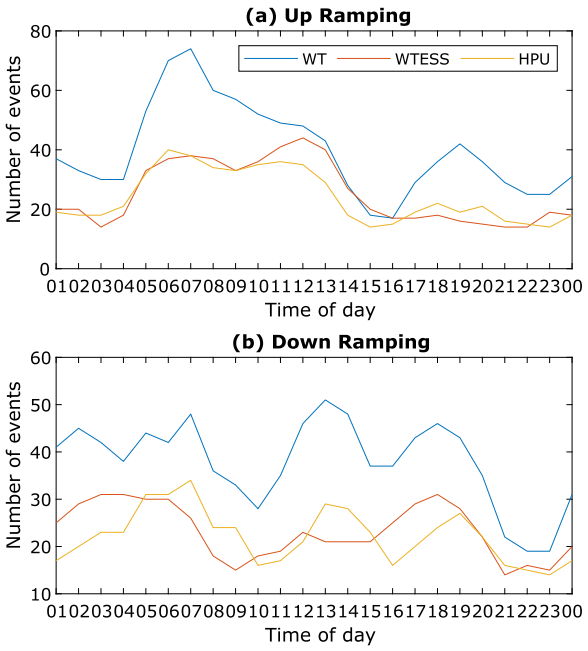

Fig. C.2. Up- and down-ramping comparison between sole WT, WT with ESS and hybrid system in 2014 at Sydney location.

The ramp characteristics of standalone WT, WTESS and the HPU system configurations are compared in Fig. C.2. It can be seen that both WTEES and HPU have a similar level/pattern of ramp mitigation effect and can significantly reduce the ramping events during all periods of the day, especially the up-ramping during the morning time when the load demand is low (see Fig. C.2 up) and the down-ramping in the evening when the demand is high (see Fig. C.2 bottom). This also validates the sizing of the EES of WT based on the equivalent smoothing effect of the HPU system.

Furthermore, a dynamic ESS model With defined energy capacity and power capacity is developed to investigate the SoC of the ESS operation during a year as shown in Fig. C.3. From Fig. C.3a, the power rate of charge and discharge satisfies 99% charge/discharge events. It is noted that, in general, ESS cannot be fully discharged or charged (known as depth of discharging) to avoid degradation issues. Therefore, the ESS should be operated within the allowable region (known as Depth of Discharge, DoD) with minimum SoC of 10% and 90% of maximum SoC, as shown in Fig. C.3(c&d).

In terms of ESS type selections, the Vanadium redox flow battery is a relatively mature technology widely applied for long-duration energy storage. However, it is not considered a solution for offshore deployment due to the low energy density, significant maintenance cost and sensitivity to ambient temperature, especially in the harsh ocean environment. The Lead–acid battery presents a higher technical maturity and a lower cost than the flow battery; however, due to the short economic life, a significantly higher replacement cost is identified among other batteries, specifically in high deep discharge (DoD) applications. In addition, the NaS (Sodium sulphur) battery is one of the most promising BES technologies for future large-scale storage systems due to its advantages, such as fast response, high power density and negligible discharge rate. However, the high cost and technical complexity (such as high-temperature reactions) are recently the main barriers to offshore applications.

Appendix D. Cost breakdown in sydney location

The cost breakdown of each generation unit for the WT, the WTESS and the HPU in an exemplary energy farm in the Sydney location is

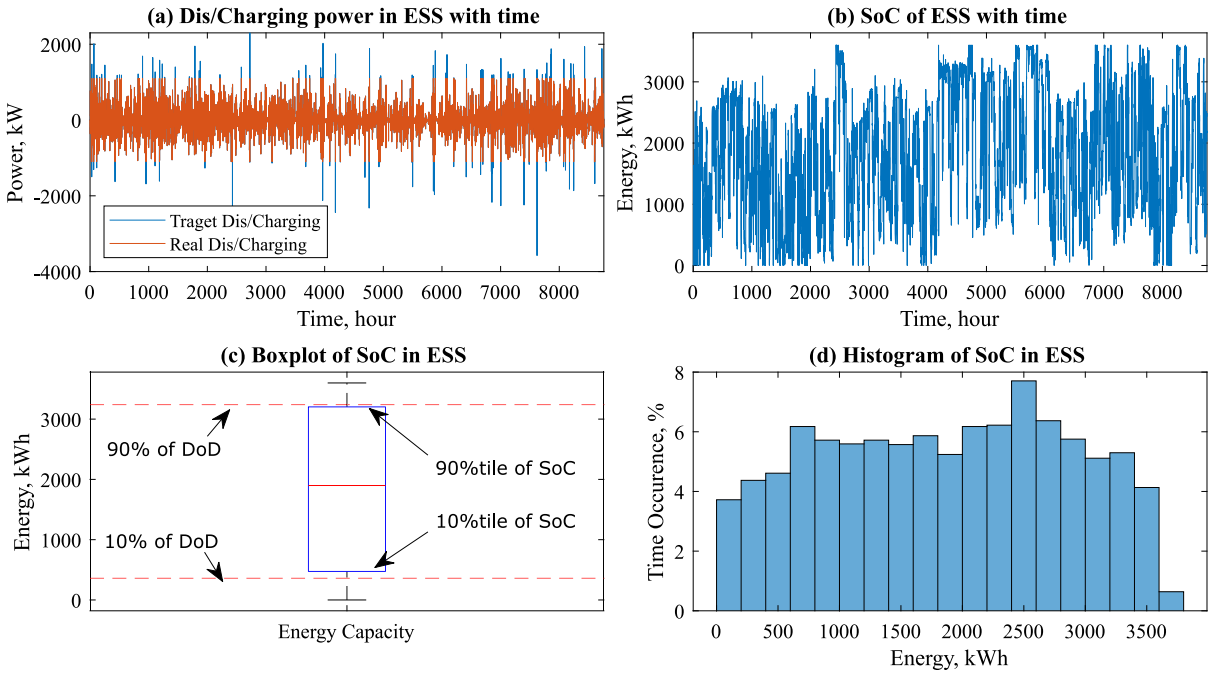

Fig. C.3. Energy Storage SOC with $P_{c/d} = 1100$ kW and $E_{ESS} = 3600$ kWh in 2014 at Sydney location.

Table D.1
The cost breakdown of per generation unit.

Cost items per generation unit			WT (k€)	WTESS (k€)	HPU (k€)
CAPEX	D&C		1,041	1,041	2,073
	C_{build}	Turbine	4,373	4,373	4,373
		Foundation	3,740	3,740	3,740
		WEC	–	–	6,000
		ESS	–	2,919	–
	$C_{install}$	Turbine	2,307	2,307	2,307
		WEC	–	–	1,157
		ESS	–	292	–
	$C_{Connection}$	Onshore sub	330	330	485
		Offshore sub	930	930	1,368
		Trans cable	929	929	1,367
		Inter-array cable	517	517	541
		WT-WEC cable	–	–	636
OPEX	$C_{O\&M}$	WT	650	650	533
		WEC	–	–	315
		ESS	–	39.4	–
	$C_{insurance}$	WT	95	95	95
		WEC	–	–	50
		ESS	–	10.8	–
	C_{admin}		47	47	69
DCPEX	Decommission		1,880	2,085	2,855
Expenditure per MW (M€/MW)			3.37	4.06	3.77
LCOE		(€/MWh)	**99.6**	**115.9**	**107.9**

shown in Table D.1. The building cost including all the generating device expenses (such as turbines, foundations, WEC and/or ESS) account for 48.2%, 54.3% and 50.5% of the total expenses allocated to each generation unit. The connection cost per generation unit accounts for 16.1%, 13.3% and 15.7% of total expenses for WT, WTESS and HPU systems, respectively. Note that the expenditure per MW of WT, WTESS and HPU systems are 3.37 M€, 4.06 M€ and 3.77M€ respectively which also follows the trend of LCOEs of these configurations. This indicates that the HPU could offer cost benefits compared to the WTESS system while providing the same level of power smoothing effect. It is also noted that the HPU may provide a more competitive cost compared to standalone WT in some other places, such as Port Lincoln in Australia and Blunt Reef in North America.

References

[1] GWEC. Global offshore wind report 2021. Technical report, Global Wind Energy Council; 2021.

[2] Pérez-Collazo C, Greaves D, Iglesias G. A review of combined wave and offshore wind energy. Renew Sustain Energy Rev 2015;42:141–53.

[3] Guo B, Ringwood JV. Geometric optimisation of wave energy conversion devices: A survey. Appl Energy 2021;297:117100.

[4] Ahamed R, McKee K, Howard I. Advancements of wave energy converters based on power take off (PTO) systems: A review. Ocean Eng 2020;204:107248.

[5] Akrami A, Doostizadeh M, Aminifar F. Power system flexibility: An overview of emergence to evolution. J Mod Power Syst Clean Energy 2019;7(5):987–1007. http://dx.doi.org/10.1007/s40565-019-0527-4.

[6] Impram S, Varbak Nese S, Oral B. Challenges of renewable energy penetration on power system flexibility: A survey. Energy Strategy Rev 2020;31:100539. http://dx.doi.org/10.1016/j.esr.2020.100539, URL https://www.sciencedirect.com/science/article/pii/S2211467X20300924.

[7] Yuan R, Pourmousavi SA, Soong WL, Nguyen G, Liisberg JA. IRMAC: Interpretable refined motifs in binary classification for smart grid applications. Eng Appl Artif Intell 2023;117:105588. http://dx.doi.org/10.1016/j.engappai.2022.105588, URL https://www.sciencedirect.com/science/article/pii/S0952197622005784.

[8] Ela E, Kemper J. Wind plant ramping behavior. Technical report december, National Renewable Energy Laboratory; 2009, URL http://www.nrel.gov/docs/fy10osti/46938.pdf.

[9] Ferreira C, Gama J, Matias L, Botterud A, Wang J. A survey on wind power ramp forecasting. Technical report, Argonne National Lab.(ANL), Argonne, IL (United States); 2011.

[10] Florita A, Hodge BM, Orwig K. Identifying wind and solar ramping events. In: IEEE green technologies conference. IEEE; 2013, p. 147–52. http://dx.doi.org/10.1109/GreenTech.2013.30.

[11] Gao Q, Ding B, Ertugrul N, Li Y. Impacts of mechanical energy storage on power generation in wave energy converters for future integration with offshore wind turbine. Ocean Eng 2022;261:112136.

[12] Li Q, Li X, Mi J, Jiang B, Chen S, Zuo L. Tunable wave energy converter using variable inertia flywheel. IEEE Trans Sustain Energy 2020;12(2):1265–74.

[13] Li B, DeCarolis JF. A techno-economic assessment of offshore wind coupled to offshore compressed air energy storage. Appl Energy 2015;155:315–22.

[14] Roy A, Kedare SB, Bandyopadhyay S. Optimum sizing of wind-battery systems incorporating resource uncertainty. Appl Energy 2010;87(8):2712–27.

[15] Ceballos S, Rea J, Robles E, Lopez I, Pou J, O'Sullivan D. Control strategies for combining local energy storage with wells turbine oscillating water column devices. Renew Energy 2015;83:1097–109.

[16] Zhao H, Wu Q, Hu S, Xu H, Rasmussen CN. Review of energy storage system for wind power integration support. Appl Energy 2015;137:545–53.
[17] International Renewable Energy Agency. Renewable power generation costs in 2020. Technical report, IRENA; 2021.
[18] Yu Y, Li Y. Preliminary results of a RANS simulation for a floating point absorber wave energy system under extreme wave conditions. Technical report, National Renewable Energy Lab.(NREL), Golden, CO (United States); 2011.
[19] Chen X, Jiang Z, Li Q, Li Y, Ren N. Extended environmental contour methods for long-term extreme response analysis of offshore wind turbines. J Offshore Mech Arct Eng 2020;142(5):052003.
[20] Wu X, Hu Y, Li Y, Yang J, Duan L, Wang T, et al. Foundations of offshore wind turbines: A review. Renew Sustain Energy Rev 2019;104:379–93.
[21] Micallef D, Rezaeiha A. Floating offshore wind turbine aerodynamics: Trends and future challenges. Renew Sustain Energy Rev 2021;152:111696.
[22] Zhang L, Li Y, Xu W, Gao Z, Fang L, Li R, et al. Systematic analysis of performance and cost of two floating offshore wind turbines with significant interactions. Appl Energy 2022;341:119341.
[23] Gao Z, Feng X, Z. Z, Liu Z, Gao X, Zhang L, et al. A brief discussion on offshore wind turbine hydrodynamics problem. J Hydrodyn 2022;34:15–30.
[24] GWEC. Global wind report 2022. Technical report, Global Wind Energy Council; 2022.
[25] Maienza C, Avossa A, Ricciardelli F, Coiro D, Troise G, Georgakis CT. A life cycle cost model for floating offshore wind farms. Appl Energy 2020;266:114716.
[26] International Renewable Energy Agency. Renewable power generation costs in 2021. Technical report, IRENA; 2022.
[27] Li Y, Yu YH. A synthesis of numerical methods for modeling wave energy converter-point absorbers. Renew Sustain Energy Rev 2012;16:4352–64.
[28] Hayward J. Wave energy cost projections. Technical report, CSIRO Energy; 2021.
[29] Commission E. Ocean energy: technology development report. Technical report, European Commission; 2019.
[30] Gao Q, Ertugrul N, Ding B, Negnevitsky M. Offshore wind, wave and integrated energy conversion systems: A review and future. In: 2020 australasian universities power engineering conference. IEEE; 2020, p. 1–6.
[31] Perez-Collazo C, Pemberton R, Greaves D, Iglesias G. Monopile-mounted wave energy converter for a hybrid wind-wave system. Energy Convers Manage 2019;199:111971.
[32] Michele S, Renzi E, Perez-Collazo C, Greaves D, Iglesias G. Power extraction in regular and random waves from an OWC in hybrid wind-wave energy systems. Ocean Eng 2019;191:106519.
[33] Si Y, Chen Z, Zeng W, Sun J, Zhang D, Ma X, et al. The influence of power-take-off control on the dynamic response and power output of combined semi-submersible floating wind turbine and point-absorber wave energy converters. Ocean Eng 2021;227:108835.
[34] Meng F, Sergiienko N, Ding B, Zhou B, Da Silva LSP, Cazzolato B, et al. Co-located offshore wind–wave energy systems: Can motion suppression and reliable power generation be achieved simultaneously? Appl Energy 2023;331:120373.
[35] Gao Q, Ertugrul N, Ding B. Method and analysis of short-term intermittency in hybrid wind and wave power unit. In: 2022 australasian universities power engineering conference. IEEE; 2022, p. 1–6.
[36] Astariz S, Iglesias G. Output power smoothing and reduced downtime period by combined wind and wave energy farms. Energy 2016;97:69–81.
[37] Gideon RA, Bou-Zeid E. Collocating offshore wind and wave generators to reduce power output variability: A multi-site analysis. Renew Energy 2021;163:1548–59.
[38] Clemente D, Rosa-Santos P, Taveira-Pinto F. On the potential synergies and applications of wave energy converters: A review. Renew Sustain Energy Rev 2021;135:110162.
[39] Astariz S, Vazquez A, Sánchez M, Carballo R, Iglesias G. Co-located wave-wind farms for improved O&M efficiency. Ocean Coast Manag 2018;163:66–71.
[40] Astariz S, Perez-Collazo C, Abanades J, Iglesias G. Co-located wind-wave farm synergies (operation & maintenance): A case study. Energy Convers Manage 2015;91:63–75.
[41] Ferrari F, Besio G, Cassola F, Mazzino A. Optimized wind and wave energy resource assessment and offshore exploitability in the Mediterranean sea. Energy 2020;190:116447.
[42] Gaughan E, Fitzgerald B. An assessment of the potential for co-located offshore wind and wave farms in Ireland. Energy 2020;200:117526.
[43] Gao Q, Khan SS, Sergiienko N, Ertugrul N, Hemer M, Negnevitsky M, et al. Assessment of wind and wave power characteristic and potential for hybrid exploration in Australia. Renew Sustain Energy Rev 2022;168:112747.
[44] Clark CE, Miller A, DuPont B. An analytical cost model for co-located floating wind-wave energy arrays. Renew Energy 2019;132:885–97.
[45] Castro-Santos L, Martins E, Soares CG. Economic comparison of technological alternatives to harness offshore wind and wave energies. Energy 2017;140:1121–30.
[46] Astariz S, Iglesias G. Selecting optimum locations for co-located wave and wind energy farms. part II: A case study. Energy Convers Manage 2016;122:599–608.
[47] Stoutenburg ED, Jenkins N, Jacobson MZ. Power output variations of co-located offshore wind turbines and wave energy converters in California. Renew Energy 2010;35(12):2781–91.
[48] CSIRO. CAWCR wave hindcast aggregated collection. 2020, https://data.csiro.au/collections/collection/CI46550 [Accessed: 30 June 2021].
[49] Hemer MA, Zieger S, Durrant T, O'Grady J, Hoeke RK, McInnes KL, et al. A revised assessment of Australia's national wave energy resource. Renew Energy 2017;114:85–107.
[50] Hersbach H, Bell B, Berrisford P, Biavati G, Horányi A, Muñoz Sabater J, et al. ERA5 hourly data on single levels from 1979 to present. In: Copernicus climate change service (C3S) climate data store, Vol. 10. ECMWF Reading, UK; 2018.
[51] Masters GM. Renewable and efficient electric power systems. John Wiley & Sons; 2013.
[52] Ertugrul N, Abbott D. DC is the future [point of view]. Proc IEEE 2020;108(5):615–24.
[53] Fusco F, Nolan G, Ringwood JV. Variability reduction through optimal combination of wind/wave resources–an Irish case study. Energy 2010;35(1):314–25.
[54] Babarit A, Hals J, Muliawan MJ, Kurniawan A, Moan T, Krokstad J. Numerical benchmarking study of a selection of wave energy converters. Renew Energy 2012;41:44–63.
[55] Wind-turbine-modelcom. Gamesa G128-5.0MW. 2021.
[56] Gamesa. Gamesa 5.0MW. 2022, https://d3pcsg2wjq9izr.cloudfront.net/files/25679/download/446231/catalogo-g10x-45mw-eng.pdf [Accessed: 01 May 2022].
[57] Xu Q, Li Y, Yu Y, Ding B, Jiang Z, Lin Z, et al. Experimental and numerical investigations of a two-body floating-point absorber wave energy converter in regular waves. J Fluids Struct 2019;91:102613.
[58] Meng F, Ding B, Sergiienko NY, Chen H, Xu H, Li Y. Power set-point tracking of a point absorber with multiple power take-off units in irregular waves. IEEE Trans Sustain Energy 2021.
[59] Zheng X, Chen G, Cao W, Xu H, Zhao R, Xu Q, et al. On the energy conversion characteristics of a top-mounted pitching absorber by using smoothed particle hydrodynamics. Energy Convers Manage 2021;250:114893.
[60] WaveStar. Wavestar prototype at roshage: performance data for ForskVE project No 2009-1-10305 phasse 1 & 2. Technical report, Wave Star A/S; 2013.
[61] Marquis L, Kramer M, Kringelum J, Chozas JF, Helstrup N. Introduction of wavestar wave energy converters at the Danish offshore wind power plant horns rev 2. In: 4th international conference on ocean energy. ICOE; 2012, p. 1–6.
[62] Gallego-Castillo C, Cuerva-Tejero A, Lopez-Garcia O. A review on the recent history of wind power ramp forecasting. Renew Sustain Energy Rev 2015;52:1148–57. http://dx.doi.org/10.1016/j.rser.2015.07.154.
[63] Fernández Á, Alaíz CM, González AM, Díaz J, Dorronsoro JR. Diffusion methods for wind power ramp detection. In: International work-conference on artificial neural networks. Springer; 2013, p. 106–13.
[64] Revheim P, Beyer H. Offshore ramp forecasting using offsite data. In: EERA deepwind 2014 deep sea offshore wind R&D conference. 2014.
[65] Gao Q, Bechlenberg A, Vakis AI, Ertugrul N, Jayawardhana B, Ding B. Techno-economic assessment of offshore wind and hybrid wind-wave farms with energy storage systems. Submitt Renew Sustain Energy Rev 2022.
[66] Orsted. Horns rev 2 offshore wind farm. 2022, https://orsted.com/ [Accessed: 30 Nov 2022].
[67] He F, Wagner M, Zhang L, Shao C, Xu W, Chen W, et al. A novel integrated approach for offshore wind power optimization. Ocean Eng 2022;266:112827.
[68] Pemberton A, Daly T, Ertugrul N. On-shore wind farm cable network optimisation utilising a multiobjective genetic algorithm. Wind Eng 2013;37(6):659–73.
[69] Aldersey-Williams J, Rubert T. Levelised cost of energy–a theoretical justification and critical assessment. Energy Policy 2019;124:169–79.
[70] Astariz S, Perez-Collazo C, Abanades J, Iglesias G. Co-located wave-wind farms: Economic assessment as a function of layout. Renew Energy 2015;83:837–49.
[71] Myhr A, Bjerkseter C, Ågotnes A, Nygaard TA. Levelised cost of energy for offshore floating wind turbines in a life cycle perspective. Renew Energy 2014;66:714–28.
[72] Bjerkseter C, Ågotnes A. Levelised costs of energy for offshore floating wind turbine concepts. Norwegian University of Life Sciences, Ås; 2013.
[73] Martinez A, Iglesias G. Multi-parameter analysis and mapping of the levelised cost of energy from floating offshore wind in the Mediterranean sea. Energy Convers Manage 2021;243:114416.
[74] Dalton GJ, Alcorn R, Lewis T. Case study feasibility analysis of the Pelamis wave energy convertor in Ireland, Portugal and north America. Renew Energy 2010;35(2):443–55.
[75] Bedard R, Hagerman G, Siddiqui O. System level design, performance and costs for San Francisco California Pelamis offshore wave power plant. San Francisco: EPRI; 2004.
[76] Têtu A, Fernandez Chozas J. A proposed guidance for the economic assessment of wave energy converters at early development stages. Energies 2021;14(15):4699.
[77] Ioannou A, Angus A, Brennan F. A lifecycle techno-economic model of offshore wind energy for different entry and exit instances. Appl Energy 2018;221:406–24. http://dx.doi.org/10.1016/j.apenergy.2018.03.143.
[78] Gonzalez-Rodriguez AG. Review of offshore wind farm cost components. Energy Sustain Dev 2017;37:10–9.
[79] Dicorato M, Forte G, Pisani M, Trovato M. Guidelines for assessment of investment cost for offshore wind generation. Renew Energy 2011;36(8):2043–51.

[80] Bosserelle C, Reddy S, Krüger J. Cost analysis of wave energy in the Pacific. Waves Coasts Pacific 2015.
[81] Estate TC. A guide to an offshore wind farm. Technical report, The Crown Estate; 2019, URL www.thecrownestate.co.uk.
[82] Jump E, Gray A, Thompson D, Stevenson L, Strang-Moran C. Offshore substations: fixed or floating? - technoeconomic analysis. Technical report, Offshore Wind Innovation Hub; 2021.
[83] Martinez A, Iglesias G. Mapping of the levelised cost of energy for floating offshore wind in the European Atlantic. Renew Sustain Energy Rev 2022;154:111889.
[84] Chamberlain K. Offshore operators act on early decommissioning – wind energy update. 2016, https://www.reutersevents.com/renewables/wind-energy-update/offshore-operators-act-early-decommissioning-data-limit-costs [Accessed: 03 June 2022].
[85] Judge F, McAuliffe FD, Sperstad IB, Chester R, Flannery B, Lynch K, et al. A lifecycle financial analysis model for offshore wind farms. Renew Sustain Energy Rev 2019;103:370–83.
[86] Castro-Santos L, Martins E, Soares CG. Cost assessment methodology for combined wind and wave floating offshore renewable energy systems. Renew Energy 2016;97:866–80.
[87] Mongird K, Viswanathan V, Alam J, Vartanian C, Sprenkle V, Baxter R. 2020 Grid energy storage technology cost and performance assessment. Energy 2020;2020.
[88] Aurecon. 2021 costs and technical parameter review. Technical report, AEMO; 2021.
[89] CATAPULT Offshore Renewable Energy. Operations & maintenance: cost drivers. Technical report, Offshore Wind Innovation Hub; 2022.
[90] Marinus. Marinus link. 2022, https://www.marinuslink.com.au/ [Accessed: 01 May 2022].
[91] Basslink. Basslink project. 2022, http://www.basslink.com.au/ [Accessed: 01 May 2022].
[92] Mongird K, Fotedar V, Viswanathan V, Koritarov V, Balducci P, Hadjerioua B, et al. Energy storage technology and cost characterization report. Technical report, U.S. Department of Energy; 2019.
[93] Graham P, Hayward J, Foster J, Havas L. GenCost 2021-22 consultation draft. Technical report, CSIRO; 2021.
[94] Chang G, Jones CA, Roberts JD, Neary VS. A comprehensive evaluation of factors affecting the levelized cost of wave energy conversion projects. Renew Energy 2018;127:344–54.
[95] Liu G, Vrakopoulou M, Mancarella P. Assessment of the capacity credit of renewables and storage in multi-area power systems. IEEE Trans Power Syst 2020;36(3):2334–44.
[96] Mosadeghy M, Saha TK, Yan R. Increasing wind capacity value in Tasmania using wind and hydro power coordination. In: 2013 IEEE power & energy society general meeting. IEEE; 2013, p. 1–5.
[97] Zhang L, Zhou Y, Flynn D, Mutale J, Mancarella P. System-level operational and adequacy impact assessment of photovoltaic and distributed energy storage, with consideration of inertial constraints, dynamic reserve and interconnection flexibility. Energies 2017;10(7):989.
[98] Zack JW. Optimization of wind power production forecast performance during critical periods for grid management. 2006.